Trabajo Fin de Máster

Máster en Ingeniería Industrial

Numerical analysis of formability and failure in tube inversion using i-Form

Autor: José Ignacio Delgado Muñoz

Tutor: Gabriel Centeno Báez

Maria Beatriz Silva (Instituto Superior Técnico, Lisboa)

Departamento de Ingeniería Mecánica y Fabricación

Escuela Técnica Superior de Ingeniería

Sevilla, 2019

Trabajo Fin de Máster

Máster en Ingeniería Industrial

Numerical analysis of formability and failure in tube inversion using i-Form

Autor:

José Ignacio Delgado Muñoz

Tutores:

Gabriel Centeno Báez

Profesor Contratado Doctor

Maria Beatriz Silva

Profesor Auxiliar

Departamento de Ingeniería Mecánica y Fabricación

Escuela Técnica Superior de Ingeniería

Universidad de Sevilla

Sevilla, 2019

Trabajo Fin de Máster: Numerical analysis of formability and failure in tube inversion using i-Form

Autor: José Ignacio Delgado Muñoz

Tutores: Gabriel Centeno Báez

Maria Beatriz Silva

El tribunal nombrado para juzgar el Proyecto arriba indicado, compuesto por los siguientes miembros:

Presidente:

Vocales:

Secretario:

Acuerdan otorgarle la calificación de:

Sevilla, Julio de 2019

El Secretario del Tribunal

Agradecimientos

A Gabriel, por su ayuda y dedicación. Por su compromiso, sus ganas de hacer las cosas bien y porque sin él no habría sido posible este trabajo.

A mi padre, ya que ha estado en todos los malos momentos.

Resumen

El trabajo se basa en un análisis numérico de tubos de Aluminio AA6063-T6 deformados con punzones de diferentes radios para el proceso de inversión. El fin principal de este trabajo consiste en determinar cuáles son los radios límites para este proceso, aumentando así el estado del arte.

El trabajo inicia con un análisis de todo lo investigado hasta ahora. Posteriormente se explica cómo ha sido modelado todo el proceso y cómo se extraen los diferentes resultados en el programa empleado: i-Form. El proceso se modela para que se lleve a cabo con una velocidad constante.

Una vez hecho esto, se pasa a exponer todos los resultados obtenidos comparándolos con resultados experimentales calculados en investigaciones anteriores, validando así los datos numéricos. Los resultados que se analizan son la fuerza y las deformaciones y, una vez validados, el daño dúctil y el espacio de la triaxialidad.

Todo esto permite definir con bastante seguridad los radios límites para llevar a cabo el proceso de inversión de forma satsifactoria tanto para radios pequeños como para radios grandes.

Abstract

The work is based on a numerical analysis of aluminum tubes AA6063-T6 deformed with punches of different radius for the inversion process. The main purpose of this work is to determine what are the radii limits for this process, increasing the state of the art.

The work begins with an analysis of everything investigated so far. Subsequently, it explains how the whole process has been modeled and how the different results are extracted in the program used: i-Form. The process is modeled to be carried out with a constant speed.

Once this is done, all the results obtained are presented, comparing them with experimental results calculated in previous investigations, validating the numerical data. The results that are analyzed are the force and the strains and, once validated, the ductile damage and the space of triaxiality.

All this allows to define with certainty the radii limits to carry out the inversion process in a satsifactory way for both small radios and large radios.

Contents

1. Introduction 1

1.1 State of the Art 2

1.2 Document structure 17

1.3 Objectives 18

2. Numerical model 19

2.1 Introduction 19

2.2 i-Form 19

2.2.1 Analytical framework 19

2.2.2 Pre-processor 22

2.2.3 Simulation process 30

2.2.4 Postprocessor 31

3. Results 37

3.1 Introduction 37

3.2 Force analysis 37

3.2.1 Small inversion radius 37

3.2.2 Large inversion radius 38

3.2.3 Intermediate inversion radius 39

3.3 Strain analysis 41

3.3.1 Small inversion radius 41

3.3.2 Large inversion radius 42

3.3.3 Intermediate inversion radius 43

3.4 Ductile damage analysis ... 46

3.5 Formability limits ... 48

3.6 Triaxiality analysis ... 50

4. Conclusions and future work ... 53

5. References ... 55

Annex A – Matlab Code ... 57

Annex B – Ductile damage and state of the tube at the beginning of the inversion ... 59

List of figures

Figure 1. Frame structure 1

Figure 2. Stress and strain of a sheet in plane stress (Análisis de los Procesos de Conformado de Chapa)..3

Figure 3. Different ways of crack propagation (T.L. Anderson)....................................4

Figure 4. Deformation paths in plane stress (Análisis de los Procesos de Conformado de Chapa) 5

Figure 5. FLD for AA6063-T6 tubes (Magrinho et al., On the Determination of Forming Limits in Thin-Walled Tubes, 2019)..6

Figure 6 (Magrinho et al., On the Determination of Forming Limits in Thin-Walled Tubes, 2019) 8

Figure 7. Tube expansion process (G. Centeno et al., On The Utilization of Circle Grid Analysis in Thin-walled Forming of Tubes, 2017)..9

Figure 8. Tube reduction process (G. Centeno et al., On The Utilization of Circle Grid Analysis in Thin-walled Forming of Tubes, 2017) 9

Figure 9. External and internal inversion process (P.A.R. Rosa et al., 2003) & (P.A. Rosa et al., 2004)..10

Figure 10. Load-shortening curve for external inversion (S.T.S Al-Hassani, W. Johnson & W.T. Lowe, 1972)...11

Figure 11. Deformed inversion specimens for 10, 6 and 4 mm inversion radii (S.R. Reid, 1993) 12

Figure 12. External inversion process (G. Centeno et al., On The Utilization of Circle Grid Analysis in Thin-walled Forming of Tubes, 2017)..13

Figure 13. Inversion process and parameters (G.S. Sekhon et al., 2003)..................14

Figure 14. Internal inversion process (P.A. Rosa et al., 2004)...................................14

Figure 15. Formability diagram (P.A. Rosa et al., 2004) 15

Figure 16. Energy absorbed with displacement (Magrinho et al., On the formability limits of thin-walled tube inversion, 2019) 17

Figure 17. Schematic representation of the rotation of axis (Cristino et al., A digital image correlation based methodology to characterize formability in tube forming, 2019).......20

Figure 18. Pre-Processor menu for modelling and meshing......................................22

Figure 19. Options for the geometry construction. 23

Figure 20. Representation of the cut tube 23

Figure 21. Refinement option for the mesh 24

Figure 22. Refinement menu..24

Figure 23. Structure needed of the file die2.dat to load in i-Form 25

Figure 24. Final model of the process..26

Figure 25. Main controls options 27

Figure 26. Dies options..27

Figure 27. Material Data and Yield Criteria 28

Figure 28. Assigning material options..29

Figure 29. Damage and Fracture controls..29

Figure 30. Initial simulation window 30

Figure 31. Ready simulation window for the process 30

Figure 32. Selection of the different graphics types 31

Figure 33. XY Graphics options 31

Figure 34. How to export the information 32

Figure 35. How to access to the surface strains..32

Figure 36. Surface strains menu 33

Figure 37. How to extract the ductile damage 33

Figure 38. Ductile damage menu 34

Figure 39. Effective Strain vs. Stress Triaxiality menu. 34

Figure 40. Evolution of the force for R=0.5 mm 38

Figure 41. Evolution of the force for R=20 mm 39

Figure 42. Evolution of the force for R=5 mm 39

Figure 43. Different stages of the successful tube inversion 40

Figure 44. . Evolution of the forces 40

Figure 45. Final state of the tube and location of the element analysed 41

Figure 46. Strain evolution for R=0.5 mm 42

Figure 47. Location of the element analysed and final position of the tube 42

Figure 48. Strain evolution for R=20 mm 43

Figure 49. Strain evolution for R=5 mm 44

Figure 50. Final state of the tube for each small inversion radius 45

Figure 51. Example of mode of failure for R=3 mm 45

Figure 52.Final state of the tube for large inversion radius 46

Figure 53. Moment in which the tube starts to invert 47

Figure 54. Elements analysed 48

Figure 55. Strain paths 49

Figure 56. FLD for R=10 mm 49

Figure 57. Space of effective strain vs stress-triaxiality 50

Figure 58. Limit cases 51

List of tables

Table 1. Critical ductile damage (Cristino et al., A digital image correlation based methodology to characterize formability in tube forming, 2019)..21

Table 2. Strain values for different displacements of the upper die............................44

Table 3. Displacement of the upper die at the beginning of the inversion and the ductile damage for each inversion radius..47

Table 4. Summary of the main results for each case in Element 596. 50

1. Introduction

Over the years, there have been done a lot of researches about sheet metal forming processes and are present in everyday life things. For example, thanks to sheet metal forming are produced parts of cars, whose worldwide production is around 100 million cars per year (D. Cooper).

However, due to different requirements in different industries such as aerospace constructions, tubes researches are getting importance in the forming field.

Nowadays, tones of tubes are produced each year. Tubes can be used both for domestic and industrial fields. The increase in the use of aluminium tubes is basically due to these factors:

- Reduced installation costs
- Minimization of system leaks
- No corrosion
- Cheaper and longer service life than copper and stainless steel
- Lighter weight

All these advantages have made the interest in tubes has increased during the last years. One of the fields where thin-walled tubes are being used is the lightweight structures which are basically designed to carry a given load. This principle is mainly used in the aerospace and automotive sectors, using the highest specific strength materials, in cranes, scaffolds or bridges (J. Jeswiet et al., 2008).

Another field where these tubes are used is in the frame structures. It can be distinguished between welded tubes, used mainly in bicycle frames, garden chairs or ski sticks and seamless tubes, which offer better mechanical properties, used in a smaller market because the increase in the cost (J. Jeswiet et al., 2008).

Figure 1. Frame structure

Finally, this kind of tubes are also present in compressed air systems, suction pipes and clear air pipes, cooling pipes, pipes for agricultural and forestry engineering… (Dietzel Hydraulik).

All this has led to the appearance of new processes like the incremental tube forming, which is a combination of an incremental tube spinning and a continuous tube bending process (C. Becker et al., 2014), invented in order to reduce the springback (when a metal is deformed, due its characteristics, it will have elastic and plastic deformation. Then, when the metal piece is removed from the tool only the plastic deformation will remain). (AutoForm: Forming Reality, s.f.)

Another innovative process is the friction-spinning, which allows the extension of existing forming limits and the production of more complex geometries compared with the conventional spinning processes (Friction-spinning - Grain structure modification and the impact on stress/strain behaviour, 2018).

1.1 State of the Art

This chapter will review the state of the art on tube forming, focusing on the main theme of the work, inversion. In order to do this, a series of basic concepts will be defined first.

Due to the manufacturing process used for tubes, it is correct to use the hypothesis existing for sheet metal forming to the tube forming. There are two main manufacturing processes:

- Seamless tubes: The tube is first a cylindrical ingot, which is heated and passed through a cylindrical die and then the hole is made through a penetrator.
- Welded tubes: The process starts with a metal sheet, which is bend to shape the tube. Then, the joins of the sheets are welded, closing the tube. (Mariño, 2015)

Keeping this in mind, it is logical to use the hypothesis of sheet metal forming, due to the second manufacturing method for tubes is starting from a sheet.

- **Plastic behaviour:**

To characterize the differences between the processes it is necessary to understand the plastic behaviour of the tube. This explanation is based on the hypothesis of an isotropic material and it is explained in the situation of a metal sheet, extrapolated to the tube.

In the vast majority of the processes, stresses which deform the sheet are those which are in the same plane as the sheet, whereas the stress in the direction of the thickness is usually zero or really small compared with the others. Because of this, it is a good simplification suppose that the sheet is deformed under general plane stress. This allows simplify the expressions of the plastic behaviour of the sheet. (Análisis de los Procesos de Conformado de Chapa)

Finally, it is supposed that elastic strains ($d\varepsilon^e$) are insignificant in comparison with the plastic strains ($d\varepsilon^p$).

$$d\varepsilon = d\varepsilon^e + d\varepsilon^p \approx d\varepsilon^p$$

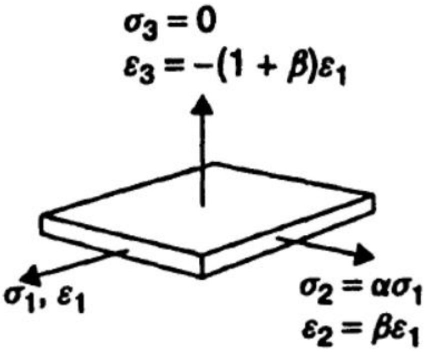
$\sigma_3 = 0$
$\varepsilon_3 = -(1+\beta)\varepsilon_1$
σ_1, ε_1
$\sigma_2 = \alpha\sigma_1$
$\varepsilon_2 = \beta\varepsilon_1$

Figure 2. Stress and strain of a sheet in plane stress (Análisis de los Procesos de Conformado de Chapa)

- **Basic relations of plasticity:**

Being axis 1 and 2 the principal strain and stress directions in the sheet plane and the axis 3, the principal direction by the thickness and supposing a general plane stress state, stress and strains existing in the sheet are:

$$\sigma_1;\ \sigma_2;\ \sigma_3 = 0$$

$$d\varepsilon_1;\ d\varepsilon_2;\ d\varepsilon_3 = -(d\varepsilon_1 + d\varepsilon_2)$$

The main direction 1 is the one in which stress is higher ($\sigma_1 > \sigma_2$). Strains $d\varepsilon_1$ and $d\varepsilon_2$ can be measured, but to calculate $d\varepsilon_3$, it is used the conservation of volume expression:

$$d\varepsilon_1 + d\varepsilon_2 + d\varepsilon_3 = 0$$

Now it can be defined two variables which are important in the following sections. These variables are α and β:

$$\alpha = \frac{\sigma_2}{\sigma_1} \qquad \beta = \frac{d\varepsilon_2}{d\varepsilon_1}$$

Where β represents the deformation path.

There is also a relation between both variables, which can be demonstrated through the Von Mises yield criterion.

This is also useful to determine the triaxiality coefficient. This criterion is expressed as follows and, considering that it is under conditions of plane stress:

$$\frac{1}{2}[(\sigma_1-\sigma_2)^2+(\sigma_1-\sigma_3)^2+(\sigma_2-\sigma_3)^2]=[1-\alpha+\alpha^2]\sigma_1^2=\sigma_Y^2$$

Where σ_Y represent the yield strength.

$$\beta = \frac{2\alpha-1}{2-\alpha} \qquad \alpha = \frac{2\beta+1}{2+\beta}$$

- **Fracture mechanics:**

Fracture mechanics is the study of how cracks start, grow and stop. It is also an important tool for improving the mechanical performance of materials and components, applying the theories of elasticity and plasticity.

There are three different ways of crack propagation:

1. **Mode I:** Opening mode: tensile stress normal to the plane of the crack, it tends to open the crack.
2. **Mode II:** Sliding mode: shear stress acting parallel to the plane of the crack and perpendicular to the crack front, it tends to slide one crack face with respect to the other
3. **Mode III:** Tearing mode: shear stress acting parallel to the plane of the crack and parallel to the crack front.

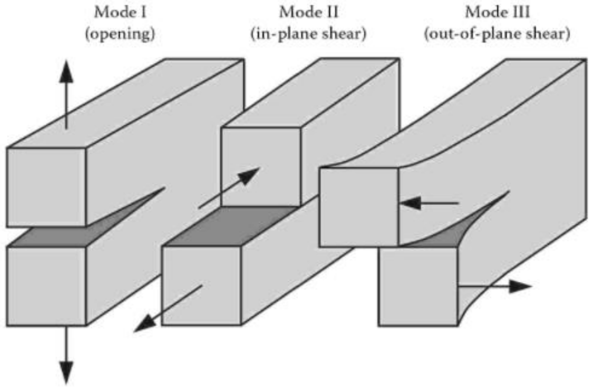

Figure 3. Different ways of crack propagation (T.L. Anderson)

A cracked body can be loaded in any of these modes or a combination of them.

- **Deformation paths in plane stress:**

The strains are usually represented in a figure during different moments of the forming process. This figure has two axes, which corresponds with the major and minor strains of the plane.

This diagram allows to obtain information about how the sheet (or tube) is deforming:

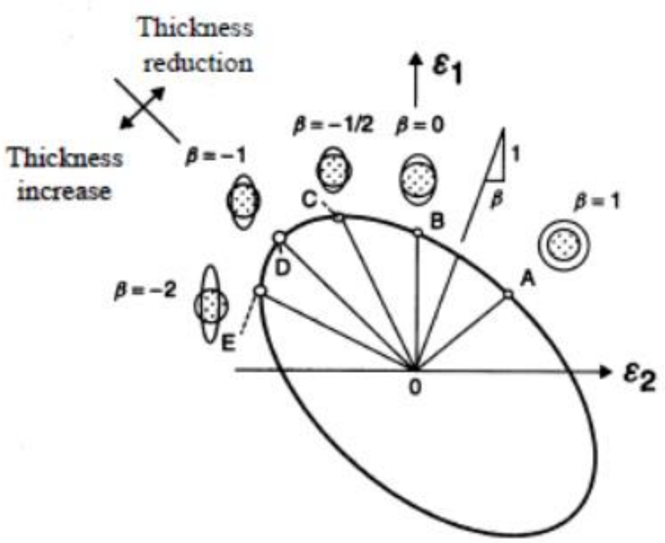

Figure 4. Deformation paths in plane stress (Análisis de los Procesos de Conformado de Chapa)

In this schematic representation, the main direction 1 is the one in which the strain (ε_1) and stress (σ_1) are higher, therefore the first point in the diagram is A, where both strains are the same ($\varepsilon_1 = \varepsilon_2$). (Análisis de los Procesos de Conformado de Chapa)

Each point in the FLC corresponds with a mechanism of deformation:

- OA: Equibiaxial expansion
- Between OA and OB there is a mechanism called biaxial tension.
- OB: Plane strain.
- OC: Uniaxial tension.
- OD: Pure shear.
- OE: Uniaxial compression.

- **Forming limit curve and fracture forming limit:**

The concept of forming limit curve (FLC) was introduced by Keeler (1964) and Goodwin (1968) and represents the first safety criterion for formability processes.

In any conformability process there is a mechanism of deformation, which can be represented in the FLC. This diagram is the most commonly used failure limit criterion in sheet metal forming industries.

Although the diagram was first used for sheet metal forming, the formability limits of thin-walled tubes were determined by (Magrinho et al., On the Determination of Forming Limits in Thin-Walled Tubes, 2019) for AA6063-T6 aluminium tubes, the material which will be utilized for the finite element analysis.

The methodology to determine the formability limit was the digital image correlation (DIC), capable to measure the strains on the vicinity of the zones where cracks are opened.

After the whole work, the researchers came to the conclusion that the FLC corresponds with the onset of necking whereas the FFL corresponds with the existence of a crack. To reach this conclusion, authors made different experiments which are widely collected in the article mentioned above. The following figure corresponds with the FLC and FFL, taken from that same article:

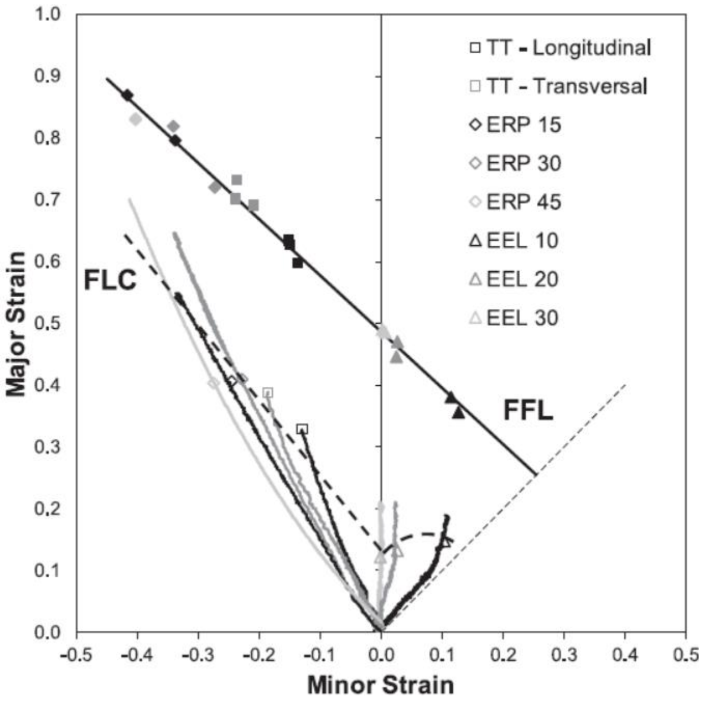

Figure 5. FLD for AA6063-T6 tubes (Magrinho et al., On the Determination of Forming Limits in Thin-Walled Tubes, 2019)

- **Triaxiality:**

Another way to characterize the fracture is the space of effective strain vs stress-triaxiality, appeared from the new forming process such as SPIF (Single point incremental forming), where local instabilities as necking are suppressed. This leads to the fracture occurring in levels of strains higher than the FFL, therefore, new limits for these processes are needed. (A.J. Martínez-Donaire et al., 2018).

J.P. Magrinho, M.B. Silva, & G. Centeno et al., 2019, researched to determine the formability limits in the space of the effective strain vs stress-triaxiality. To do this, the first thing was to measure the surface strains using the DIC methodology (Digital Image Correlation).

To calculate the value of the strains at the fracture, it is measured the thickness of the tube and the minor strain, ε_2, corresponding with the meridional stain, is supposed to remain constant after the fracture and, finally, by means of the hypothesis of incompressibility, the major strain (corresponding with the circumferential direction) can be calculated.

Once the strains are defined, the authors calculated the effective strain $\overline{\varepsilon}$, the effective stress $\overline{\sigma}$ and the average stress σ_m, using the non-quadratic plasticity criterion proposed by Hosford, derived from anisotropic sheet metals:

$$r_0(\sigma_2-\sigma_3)^a + r_{90}(\sigma_3-\sigma_1)^a + r_0 r_{90}(\sigma_1-\sigma_2)^a = r_{90}(1+r_0)\overline{\sigma}_a$$

where 1,2 and 3 correspond with the axes of anisotropy and r_0 and r_{90} with the anisotropy coefficients at 0º and 90º.

After the authors imposed plane stress conditions and tubes with FCC crystal structure, the expressions of effective strain and stress-triaxiality ratio were reduced to:

$$d\overline{\varepsilon} = \frac{1+\alpha\beta}{\left[\dfrac{r_{90}+r_0\alpha^8+r_0 r_{90}(1-\alpha)^8}{r_{90}(1+r_0)}\right]^{1/8}} d\varepsilon_1$$

$$\eta = \frac{\sigma_m}{\overline{\sigma}} = \frac{(1+\alpha)\left[r_{90}(1+r_0)\right]^{1/8}}{3\left[r_{90}+r_0\alpha^8+r_0 r_{90}(1-\alpha)^8\right]^{1/8}}$$

Where $r_0 = r_{90} = 1$.

Finally, the stress-triaxiality allowed to determine the formability limits successfully, presented in the next figure:

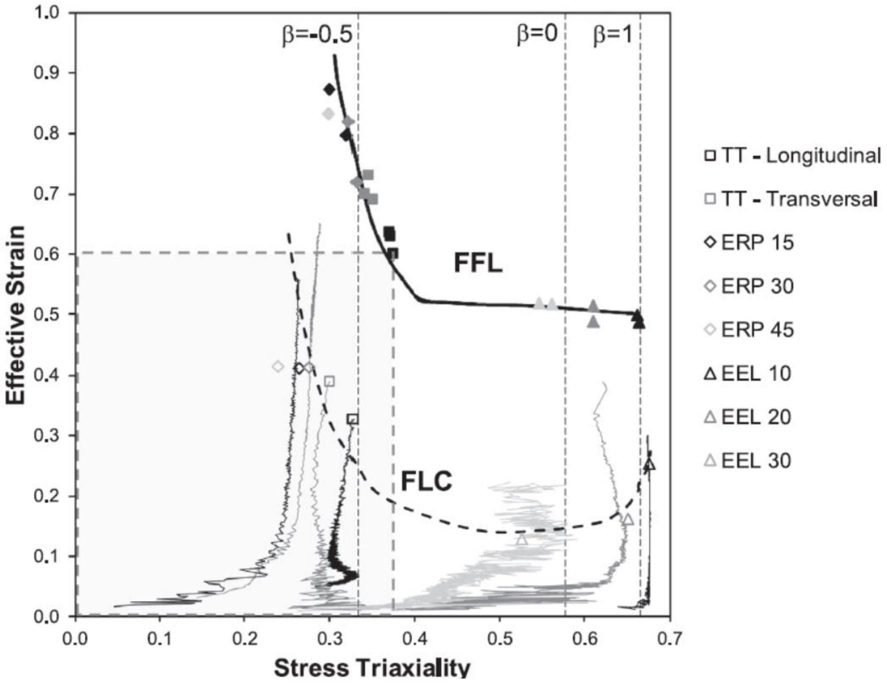

Figure 6 (Magrinho et al., On the Determination of Forming Limits in Thin-Walled Tubes, 2019)

- **Tube forming:**

Tube forming can be defined in some different ways, however, all these different definitions have something in common: the maximum strain level that a material can accept without occurring instabilities. There are different processes of tube forming, such as extrusion, forging, rolling… Within this document the only process studied will be extrusion, divided in three sub processes: expansion, reduction and inversion.

  - Expansion:

The aim of this process is increase the diameter of the tube gradually, forcing the end of the tube on a die with a determined angle.

The procedure of the expansion consists in locate the tube in the upper part of the die, where its diameter coincides with the internal diameter of the tube; then the upper plate of the press begins to go down at a constant velocity and push the tube against the die.

During this process, the tube is deformed and it takes the shape of the die. The strain produced in the tube is larger as the angle of the die increases.

The expansion of tubes has important parameters, which are shown in the next figure:

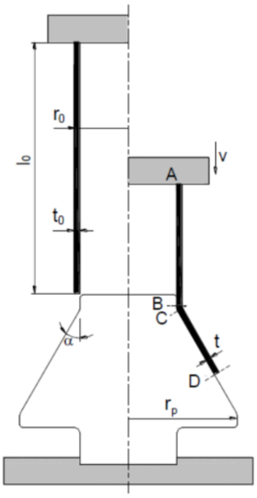

Figure 7. Tube expansion process (G. Centeno et al., On The Utilization of Circle Grid Analysis in Thin-walled Forming of Tubes, 2017)

Where r_0, t_0 and l_0 corresponds with the initial radius, thickness and length. The parameter r_p is the final radius (which is larger than the initial one), α is the angle of the die and t is the final thickness of the tube.

- Reduction:

As opposed to the expansion process, during the reduction the objective is decrease the tube diameter. In this case, the initial diameter of the lower die is larger than the final one, therefore, the angle of the die will be the symmetric with respect to the expansion one.

The rest of the process is the same as in the expansion (the unique difference is the die).

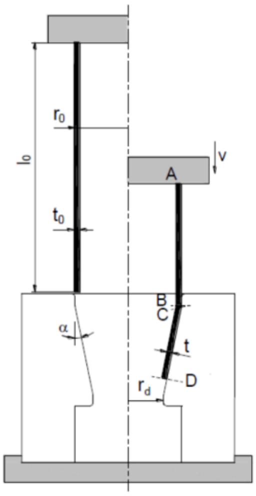

Figure 8. Tube reduction process (G. Centeno et al., On The Utilization of Circle Grid Analysis in Thin-walled Forming of Tubes, 2017)

In this case, all the parameters match with the expansion ones, except r_d which is now the final radius of the die.

- Inversion:

Although the inversion process also consists of pushing the tube against a die, it differs from expansion and reduction in that the lower die used in this process has at the top the same diameter as the internal diameter of the tube and then it has an inversion radius (not an angle).

There are two different types of inversion:

- External inversion (P.A.R. Rosa et al., 2003)
- Internal inversion (P.A. Rosa et al., 2004)

The difference between both of them is the orientation of the radius as it is shown in the Figure 9:

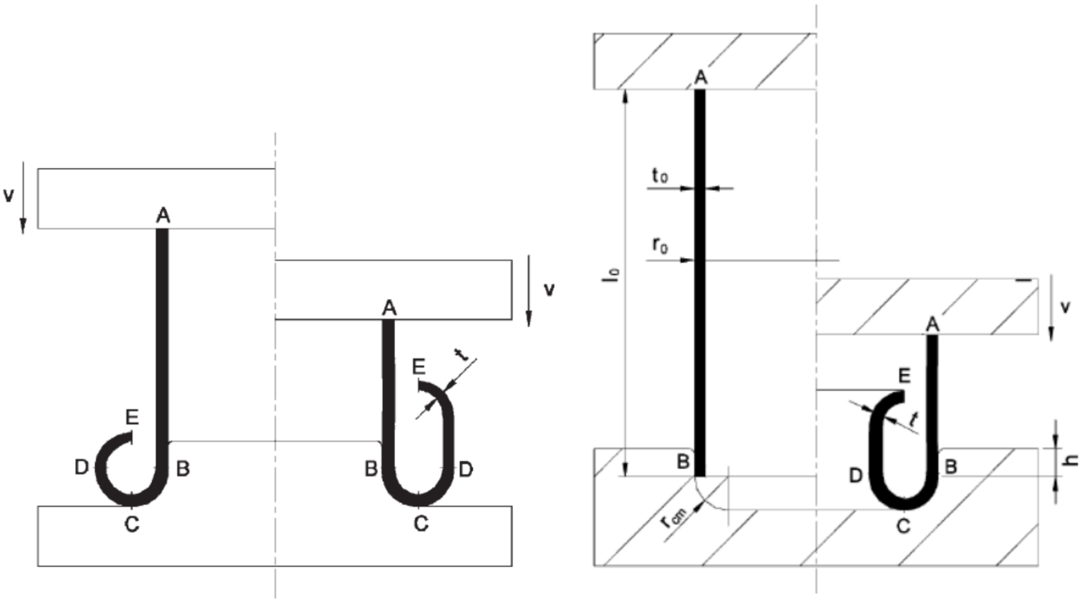

Figure 9. External and internal inversion process (P.A.R. Rosa et al., 2003) & (P.A. Rosa et al., 2004)

In both process the plastic deformation is the result of the bending, stretching and friction of the tube (P.A.R. Rosa et al., 2003). The process can be summarized as follows:

- Bending: Point B
- Friction: Between point B and C
- Unbending: Point D

The first characterization for inversion, to author’s knowledge, was taken place in S.T.S Al-Hassani, W.Johnson & W.T. Lowe, 1972, when energy absorbers were taking importance due to the motor vehicle industry, where it was difficult to protect a passenger from the deceleration pulses experienced in collisions.

In fact, inversion tube was a very interesting energy absorbing column and it was introduced in cars by General Motors three years before. Later, it was the NASA (National Aeronautics and Space Administration) which made researches to introduce them in the space vehicles to obtain softer landings.

It was the first time that the stages of the inversion were described in force terms, shown in the next figure:

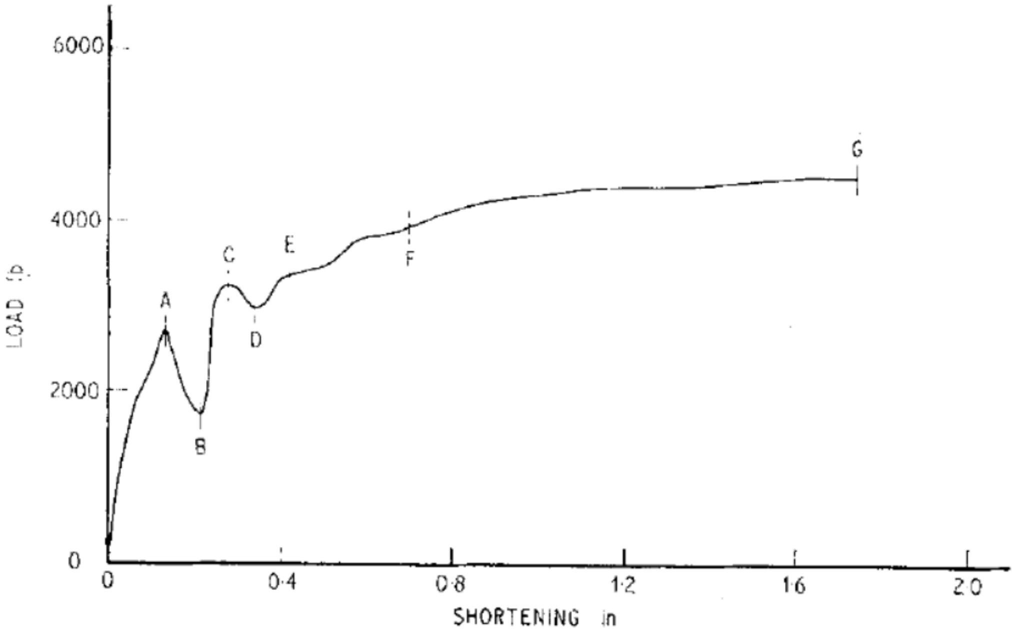

Figure 10. Load-shortening curve for external inversion (S.T.S Al-Hassani, W. Johnson & W.T. Lowe, 1972)

It is described an increase in the load until a peak A, where the tube first touches the inversion radius. Here the load decrease until the tube has adopted completely the shape of the inversion radius of the die (Point B). Then the load increase again until the tube starts the inversion (Point C). Now, the load decreases a bit until the tube has invert 180º (Point D). Finally, the load increases until the tube inverts 270º (Point E).

What was made within this research was to study the material properties, die angle, die radius, the rate of deformation and the deceleration rate. Due to there were not defined limits or effect of damage, the conclusions achieved were not very extensive, only the range of die angles were the inversion was successful (between 75º and 120º). Even so, it was a first step for inversion research in tubes

It was S.R. Reid, 1993, one of the first to determine some limits in the inversion process. His research to find energy absorbers led him to do different experiments as progressive buckling, inversion and splitting produced by axial compression.

The experiments were done with tubes of 100 mm length and the dies used had inversion radii of 3.2, 4, 6 and 10 mm. The results were that the inversion was successful for 4 and 6 mm dies, with the 3.2 mm die, the tube inverted but the bottom extreme of the tube crashed with the tube and for the 10 mm die, the tube expanded, provoking a crack.

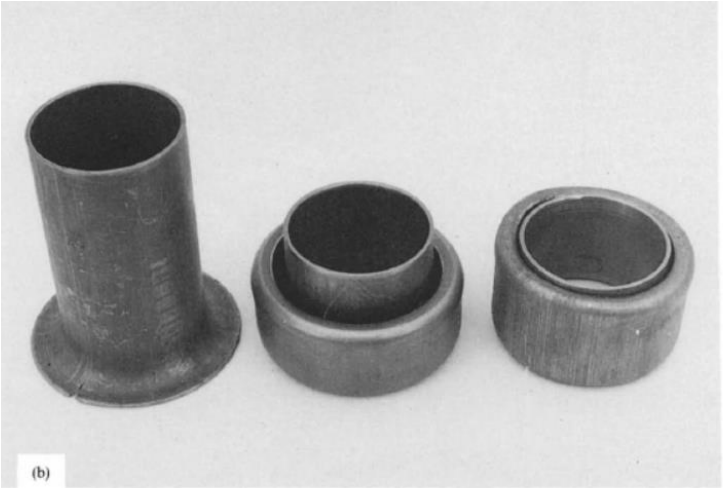

Figure 11. Deformed inversion specimens for 10, 6 and 4 mm inversion radii (S.R. Reid, 1993)

Later, P.A.R. Rosa et al., 2003, carried out a deeper research about the external inversion process with the objective of augmenting the knowledge about this process and issues related with friction and deformation modes. It was done by means of a numerical and experimental investigation.

The objective in this work was to characterize the deformation modes associated with the formability limits and the influence of the lubrication, performed on Aluminium Al6060 tube of 70 mm length. The internal radius of the tube was 18 mm in all cases and the thickness varied from 0.5 to 2 mm. Moreover, the inversion radius of the die includes radii between 2 and 10 mm.

In this article is analysed the critical instability load (which was fixed in 47.2 kN) by the axial compression of tubes, the external inversion of the tube, the load-displacement figure where the three phases of the successfully inversion process were distinguished: axial compression stage, transient invert-forming and steady-state invert forming.

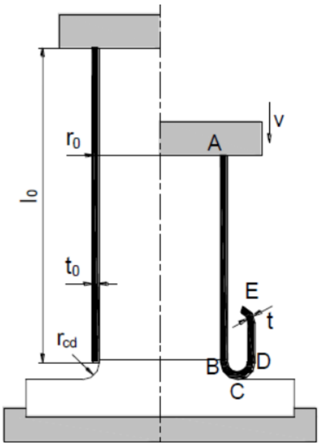

Figure 12. External inversion process (G. Centeno et al., On The Utilization of Circle Grid Analysis in Thin-walled Forming of Tubes, 2017)

The ductile damage criterion used was the Cockcroft-Latham and it was observed that for an inversion radius of 5 mm ($r_{cd}/r_0=0.278$) the accumulated damage was higher than the critical value and no cracks appeared. However, for inversion radius of 10 mm ($r_{cd}/r_0=0.556$), cracks were observed.

That is why the first forming limits mentioned are buckling for r_{cd}/r_0 low ratios (around 0.21) and cracking around the circumference for r_{cd}/r_0 high values (around 0.42).

It was determined that the lubrication is very important, promoted also due to the air that remains inside the tube and enclosed by the dies. Another conclusion reached was that using the ductile damage to study the appearance of cracks in this process was not recommendable, due to cracks were controlled by the decrease of thickness in the tube.

Also during the year 2003 G.S. Sekhon et al. carried out an analysis of the inversion process. In this case, the tubes were longer (80, 100 and 100 mm length) and thicker (1.12, 1.68 and 1.3 mm respectively). It was used a finite element software, FORGE2, to compare the experimental results with the computational model.

In this occasion, the parameters analysed were the key dimensions of the tube, defined in this work as b_e, external diameter of the inverted tube, and b_i, the diameter of the bottom extreme of the inverted tube, shown in the Figure 13. Inversion process and parameters . It was observed that b_e and *bi* increased when the inversion radius increased.

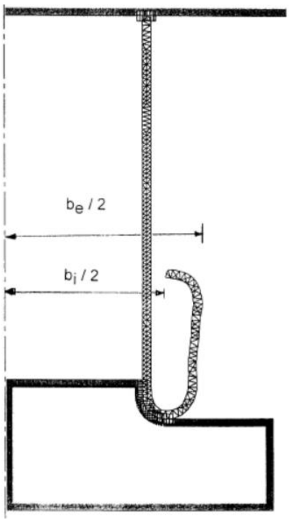

Figure 13. Inversion process and parameters (G.S. Sekhon et al., 2003)

The most important conclusions reached were that during the inversion process there were two unloads, the energy absorbed was larger for small inversion radius of the die, the friction decreased notably the capacity to absorb energy and finally that there was a friction value which made the inversion impossible.

All these advances were achieved for external inversion of the tube. It was in 2004 when P.A. Rosa et al. focused in the internal inversion, due to the external inversion was well established. It was based on the fact that both parameters and the lubrication conditions were well defined, as well as the deformation modes that would probably occur.

The objective was to determine the formability diagrams taking into account the major parameters of the process (thickness of the tube and inversion radius of the die) and also study the influence of the frictional conditions. This study was done in a theoretical and a experimental way.

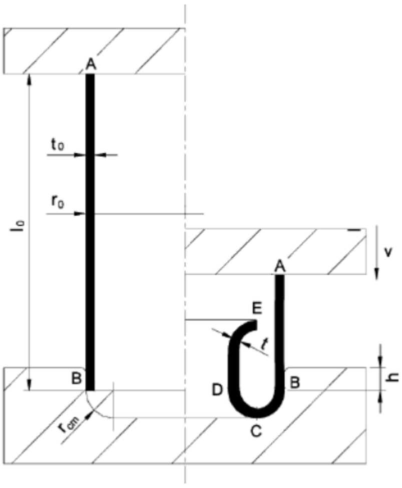

Figure 14. Internal inversion process (P.A. Rosa et al., 2004)

The tubes used were 70 mm length and the thickness were 1 or 2 mm. The inversion radius varied from 2 to 6 mm and it was done with two different materials: Al6060 (Aged) and Al6060 (Annealed).

The results obtained after doing all the experiments are collected in the following forming diagram, which shows the relative load P/P_{cr} as a funtion of the ratio r_{cd}/r_0, with a fixed thickness of 1 mm and a value of h=30 mm (see Figure 14).

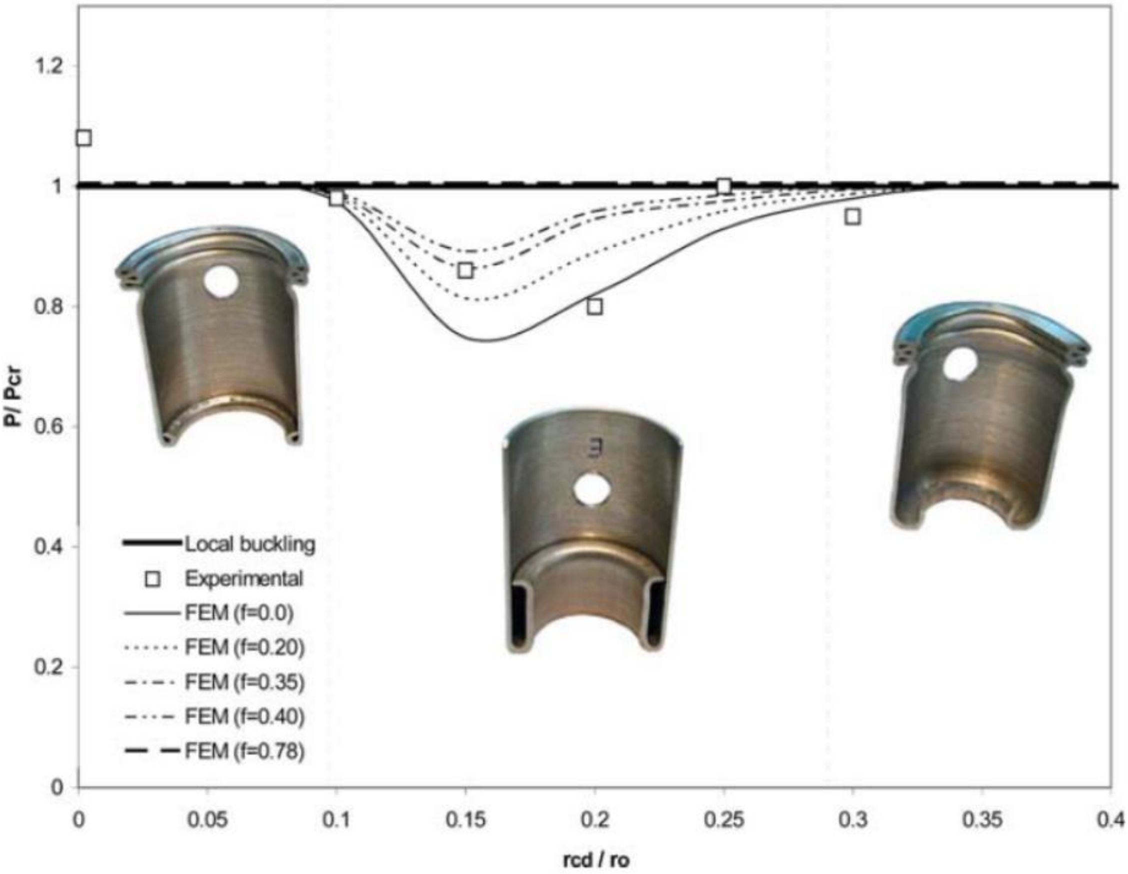

Figure 15. Formability diagram (P.A. Rosa et al., 2004)

As it happened for external inversion, explained in P.A.R. Rosa et al., 2003, low values of r_{cd}/r_0 produced buckling, whereas high values provoked wrinkling and in some situations, cracks. It was also appreciate that the lubrication had an important role in the success of the process as well as the parameter *h.*

It has been in the last year when the biggest advances have been achieved in this field, thanks to Magrinho et al., 2019, which has not yet been published since it is under review.

In that document are used new methodologies, previously applied for sheet metal forming and, later, in tube expansion. The objective here was to analysed the formability limits by local buckling, necking and fracture during the external tube inversion. For this, it was used the combination of digital image correlation (DIC) for the strains, thickness measurements, force evolution and finite element modelling.

For the research AA6063-T6 aluminium tubes were used, with 70 mm length, 18 mm of internal radius and 2 mm of thickness. Thanks to previous investigations performed by the authors for expansion process of the same tubes the mechanical properties (G. Centeno et al., Towards the characterization of fracture in thin-walled tube forming, 2016) and FLD were defined (J.P. Magrinho, M.B. Silva, & and G. Centeno et al., 2019).

To analyse the formability limits, it was defined three different inversion radii: *0.5, 5* and *20 mm*, in order to capture the entire range and, thus, have all the possibilities of evolution of the process possible previously described.

For the *R=0.5 mm* case, it was proven that the evolution of the strains corresponded at the beginning with $\beta=-2$ (pure compression) and that there were two phases:

1. Compression along the meridional direction and stretching along the circumferential direction.
2. Stretching along the meridional and circumferential direction.

For the *R=5 mm* case, it was checked the evolution in terms of forces that S.T.S Al-Hassani, W.Johnson, & W.T. lowe described in 1972. Moreover, in terms of strains, the evolution follows approximately the $\beta=-0.5$ line (pure tension) there were defined two different phases as well:

1. Compression along the meridional direction and stretching along the circumferential direction until the tube inverts.
2. Steady-state values

Finally, for the *R=20 mm* case, it was also verified what was defined before, failure due to the necking followed by cracks. The strain evolution corresponds also with $\beta=-0.5$ and only one phase was identified: increase in the load and compression along the meridional direction and stretching along the circumferential direction until the fracture of the tube.

Therefore, the conclusions reached are that within the inversion process there are three possibilities:

- Local buckling for small inversion radii
- Successful inversion for intermediate radii
- Necking for large inversion radii

Moreover, it is shown that in terms of absorbed energy, the biggest value is for the successful inversion, allowing to absorb a lot of energy during large displacements. The smallest value is for small radii, but still allows to absorb relatively high energy in small displacements. Lastly, it is concluded that large inversion radii can be used as a mechanical fuse, absorbing a fixed amount of energy for a specific displacement.

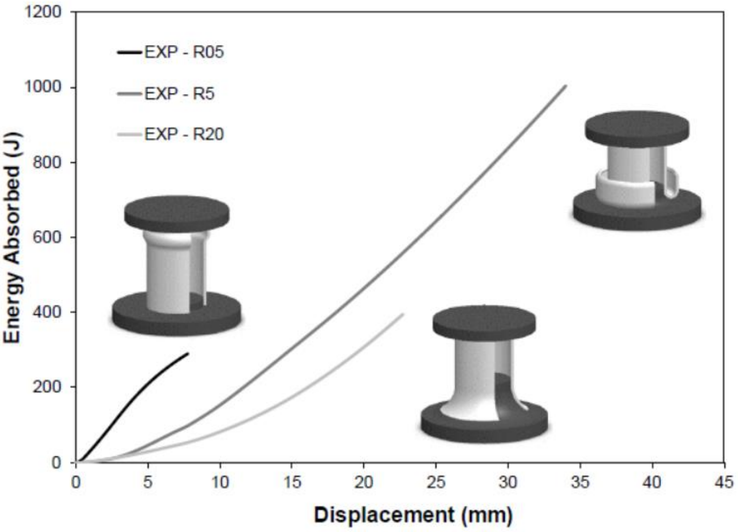

Figure 16. Energy absorbed with displacement (Magrinho et al., On the formability limits of thin-walled tube inversion, 2019)

1.2 Document structure

This document follows a structure trying to make itself comprehensive even for those who has never heard anything about tube end forming.

That is why, in the first place, there is a state of the art which includes the main concepts of formability, explaining the plastic behaviour of the material, the plasticity relations and the forming limit diagram. Furthermore, all the advances about inversion will be described to locate the starting point of this work.

Subsequently, it will be described how the software works in each of its modules. Special emphasis will be placed on the procedure followed in order to understand how the model has been generated and how the results have been obtained, so that anyone is able to carry it out.

Finally, the results obtained will be exposed in terms of forces, surface strains, ductile damage and triaxiality, followed by the conclusions obtained from the analysis of them.

1.3 Objectives

Once it has been demonstrated the effect of the inversion radius, the main objective of this document is to is to determine the radii that characterise the formability limits for the inversion process through a numerical software. This software is i-Form, which will be explained in the following sections.

To achieve this target, it will be analysed the force evolution within the inversion process depending on the inversion radius, as well as the surface strains, ductile damage and triaxiality by the use of a finite element analysis.

Taking into account all these results, it can be determined how it is expected that the tube behaves depending on the inversion radius of the die.

2. Numerical model

2.1 Introduction

The aim of this section is to define which is the software employed, how it works to carry out the inversion processes and how it is modeled.

The simulation will be carried out for tubes of 70 mm length, with an external radius of 20 mm and a thickness of 2 mm. The material used for the simulations is Aluminium AA6063-T6.

There have been performed several experimental researches for this material, allowing to have well defined the FLC and FFL, as indicated in the previous section.

2.2 i-Form

i-Form is a software developed by the *Instituto Superior Técnico of Lisboa* and the Technical University of Denmark. This program allows to make simulations in 2D of different modelling processes.

2.2.1 Analytical framework

The finite element analysis is based on the irreducible finite element flow formulation (Cristino et al., A digital image correlation based methodology to characterize formability in tube forming, 2019):

$$\prod = \int_V \bar{\sigma}\,\dot{\bar{\varepsilon}}\,dV + \frac{1}{2}K\int_V \dot{\varepsilon}_V^2 dV - \int_{S_T} T_i\,u_i\,dS + \int_{S_T}\left(\int_0^{|u_r|}\tau_f\,du_r\right)dS$$

Where:

$\bar{\sigma}$: effective stress

$\dot{\bar{\varepsilon}}$: effective strain rate

$\dot{\varepsilon}_V$: volumetric strain rate

K : large positive constant imposing the material incompressibility constraint

T_i : surface tractions

u_i : surface velocities

S_T : target surface

u_r : relative sliding velocity

τ_f : friction shear stress

S_f : contact interface between the tube and the die

V : volume

As it is explained in this article, the results that the program provides are in global coordinates (*x, y, z*), so it is necessary to rotate the strain tensor into the local coordinate system.

To do this, it is required to make two rotations: one, rotating the axes (*x, y, z*) so they coincide with the axes (*θ*, *r, z*) and the second, rotating the (*θ*, *r, z*) axis, making it coincide with axis (t, *θ*, *ϕ*), where axis *t* is perpendicular to the tube thickness and axis (*θ*, *ϕ*) are the in-plane axis, *θ* in the circumferential direction and *ϕ* in the meridional one. In order to make this more comprehensive, here can be found the mathematical expression and the graphic representation:

$$\varepsilon_{t,\theta,\phi} = R_2^T \varepsilon_{r,\theta,z} R_2 = R_2^T \left(R_1^T \varepsilon_{x,y,z} R_1 \right) R_2$$

$$R_1 = \begin{pmatrix} \cos\nu & \sin\nu & 0 \\ -\sin\nu & \cos\nu & 0 \\ 0 & 0 & 1 \end{pmatrix} \qquad R_2 = \begin{pmatrix} \cos\varpi & 0 & \sin\varpi \\ 0 & 1 & 0 \\ -\sin\varpi & 0 & \cos\varpi \end{pmatrix}$$

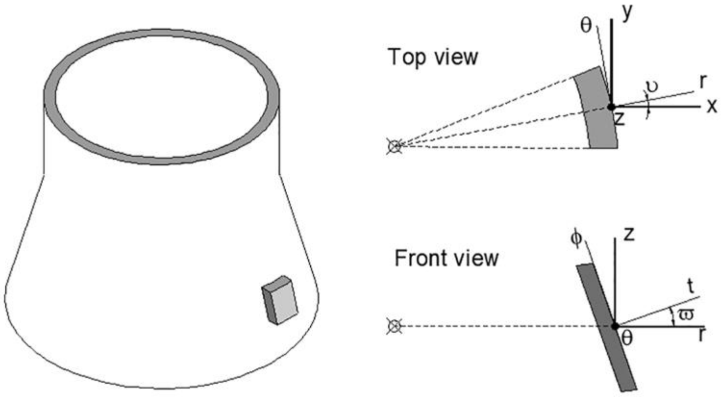

Figure 17. Schematic representation of the rotation of axis (Cristino et al., A digital image correlation based methodology to characterize formability in tube forming, 2019)

To evaluate the damage, the chosen criterion will be the void-growth damage-based one, proposed by McClintock, and utilized in several articles evaluating the fracture limit within (almost completely) tube expansion, due to the crack in expansion opens by tension (mode I of fracture mechanics) (as in Cristino et al., A digital image correlation based methodology to characterize formability in tube forming, 2018, J.P. Magrinho, M.B. Silva, & and G. Centeno et al., 2019, Cristino et al., Theory of single point incremental forming of tubes, 2019 (under review)). This will allow to make comparisons between the analytical results obtained for inversion and these obtained before.

This criterion expresses the damage in function of the effective strain, $\bar{\varepsilon}$, and the stress-triaxiality, $\sigma_m / \bar{\sigma}$ and allows determining the critical ductile damage at the onset of failure by necking.

Taking the expressions deducted by Cristino et al., Theory of single point incremental forming of tubes, 2019 (under review), it is possible to express the ductile damage in function of the strain ratio β. The hypothesis done is working under plane stress which translated into equations corresponds with:

$$\sigma_t = 0$$

If this restriction is introduced in the equations of effective stress, $\bar{\sigma}$, and effective strain increment, $d\bar{\varepsilon}$, it is obtained the following:

$$\frac{\sigma_m}{\bar{\sigma}} = \frac{1}{\sqrt{3}} \frac{1+\beta}{\sqrt{1+\beta+\beta^2}} \qquad \bar{\varepsilon} = \frac{2}{\sqrt{3}} \sqrt{1+\beta+\beta^2}\, \varepsilon_\phi$$

$$D_{crit} = \frac{2}{3}\left(1+\beta\right)\varepsilon_\phi^f$$

Where the term ε_ϕ^f corresponds with the meridional strain at the moment of the fracture.

Moving back to the research of Cristino et al., 2018, in the next table it is shown the critical values of ductile damage at the onset of failure, comparing the analytical and experimental results obtained for the different geometries.

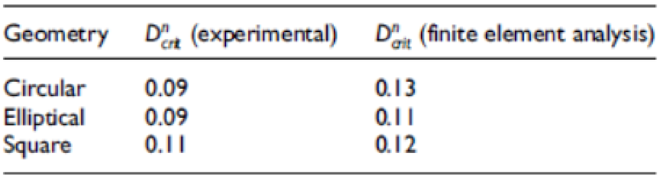

Geometry	D^n_{crit} (experimental)	D^n_{crit} (finite element analysis)
Circular	0.09	0.13
Elliptical	0.09	0.11
Square	0.11	0.12

Table 1. Critical ductile damage (Cristino et al., A digital image correlation based methodology to characterize formability in tube forming, 2019)

For the cases that will be studied in this document, the most important ductile damage value is the obtained for the circular geometry, due to is the geometry that most resembles to those of inversion although the critical value of 0.13 has been studied later and defined in a new value of 0.15

2.2.2 Pre-processor

The pre-processor menu is in charge of generating the model and mesh, assigning the material and defining the characteristics and the duration of the problem. Now, it will be explained in each section how to set all this data.

2.2.2.1 Modelling and meshing

There are two different possibilities to create the model, one is creating with the program interface and the other one, taking the data from a text file.

On the one hand, due to the fact that the tube in 2D remains as a rectangle, the tube is created using the program interface as follows:

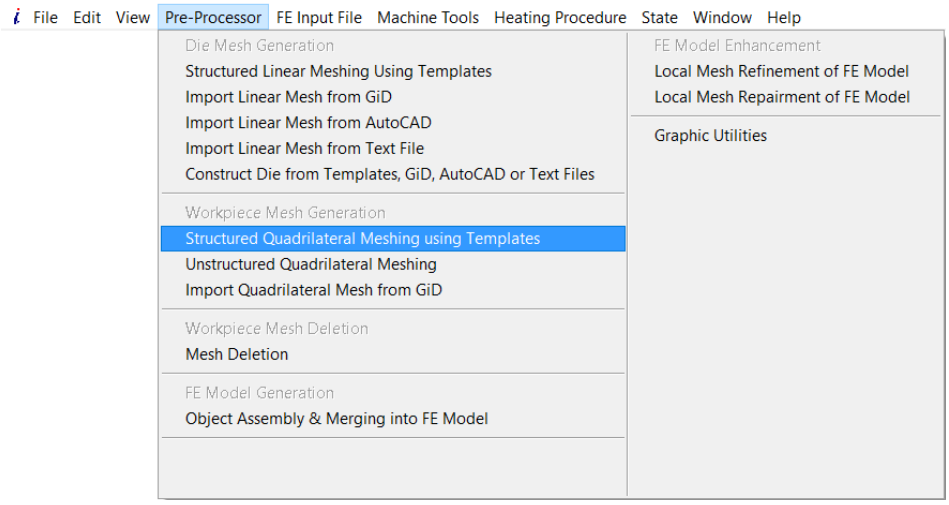
File
Edit
View
Pre-Processor
FE Input File
Machine Tools
Heating Procedure
State
Window
Help
Die Mesh Generation
Structured Linear Meshing Using Templates
Import Linear Mesh from GiD
Import Linear Mesh from AutoCAD
Import Linear Mesh from Text File
Construct Die from Templates, GiD, AutoCAD or Text Files
Workpiece Mesh Generation
Structured Quadrilateral Meshing using Templates
Unstructured Quadrilateral Meshing
Import Quadrilateral Mesh from GiD
Workpiece Mesh Deletion
Mesh Deletion
FE Model Generation
Object Assembly & Merging into FE Model
FE Model Enhancement
Local Mesh Refinement of FE Model
Local Mesh Repairment of FE Model
Graphic Utilities

Figure 18. Pre-Processor menu for modelling and meshing

Once it has been selected the option *"Structured Quadrilateral Meshing using Templates"* to create the tube, the next menu appears:

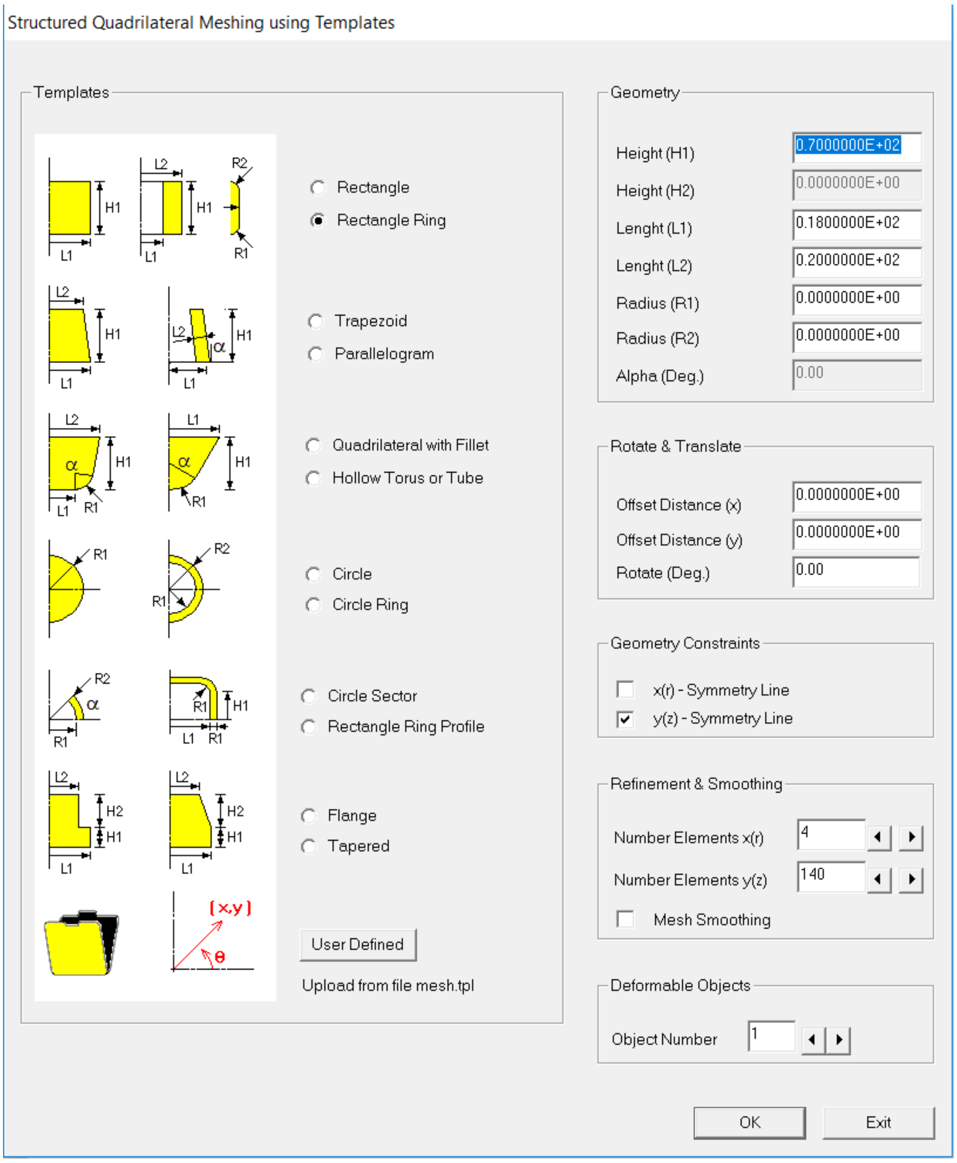

Structured Quadrilateral Meshing using Templates

Templates

○ Rectangle
● Rectangle Ring
○ Trapezoid
○ Parallelogram
○ Quadrilateral with Fillet
○ Hollow Torus or Tube
○ Circle
○ Circle Ring
○ Circle Sector
○ Rectangle Ring Profile
○ Flange
○ Tapered

Upload from file mesh.tpl

Geometry

Height (H1) 0.7000000E+02
Height (H2) 0.0000000E+00
Lenght (L1) 0.1800000E+02
Lenght (L2) 0.2000000E+02
Radius (R1) 0.0000000E+00
Radius (R2) 0.0000000E+00
Alpha (Deg.) 0.00

Rotate & Translate

Offset Distance (x) 0.0000000E+00
Offset Distance (y) 0.0000000E+00
Rotate (Deg.) 0.00

Geometry Constraints

☐ x(r) - Symmetry Line
☑ y(z) - Symmetry Line

Refinement & Smoothing

Number Elements x(r) 4
Number Elements y(z) 140
☐ Mesh Smoothing

Deformable Objects

Object Number 1

Figure 19. Options for the geometry construction.

As it was mentioned before, the 2D representation of a cut tube remains as two rectangles, one in each side of the symmetry axis:

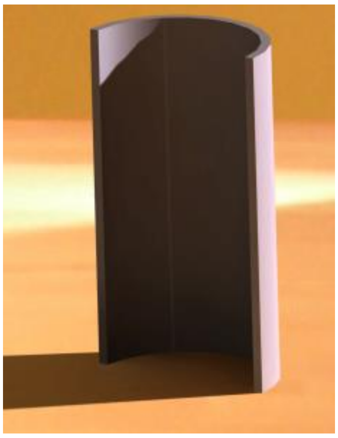

Figure 20. Representation of the cut tube

Taking this into account, the template used will be the *“Rectangle Ring”*. In the *“Geometry”* section, the height of the tube is 70 mm, the inner radius corresponds with *“Length (L1)”* will be 18 mm and the outer radius *“Length (L2)”* will be 20 mm.

In *“Geometry Constraints”* the only symmetry axis is the Y axis.

Moving now to the *“Refinement & Smoothing”* section, it has been considered that it will be enough to have two elements per millimetre in each direction, therefore, in the X direction (which has 2 mm), the number of elements chosen is 4 and in the Y direction (which has 70 mm), the number of elements is 140. This will change in the half of the tube that is deformed in order to obtain more accurate results.

To finish with the modelling of the tube, the mesh refinement mentioned before will be carried out as follows:

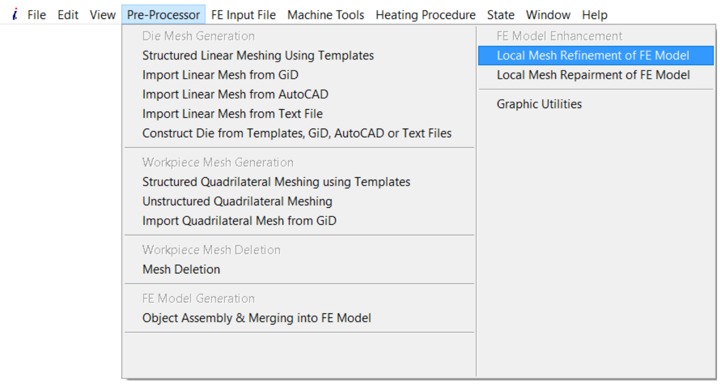
File
Edit
View
Pre-Processor
FE Input File
Machine Tools
Heating Procedure
State
Window
Help
Die Mesh Generation
Structured Linear Meshing Using Templates
Import Linear Mesh from GiD
Import Linear Mesh from AutoCAD
Import Linear Mesh from Text File
Construct Die from Templates, GiD, AutoCAD or Text Files
Workpiece Mesh Generation
Structured Quadrilateral Meshing using Templates
Unstructured Quadrilateral Meshing
Import Quadrilateral Mesh from GiD
Workpiece Mesh Deletion
Mesh Deletion
FE Model Generation
Object Assembly & Merging into FE Model
FE Model Enhancement
Local Mesh Refinement of FE Model
Local Mesh Repairment of FE Model
Graphic Utilities

Figure 21. Refinement option for the mesh

Once that option has been selected, the next menu appears:

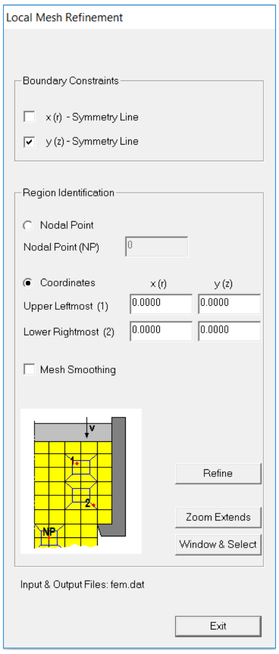
Local Mesh Refinement

Boundary Constraints

☐ x (r) - Symmetry Line
☑ y (z) - Symmetry Line

Region Identification

○ Nodal Point
Nodal Point (NP): 0

● Coordinates

	x (r)	y (z)
Upper Leftmost (1)	0.0000	0.0000
Lower Rightmost (2)	0.0000	0.0000

☐ Mesh Smoothing

Input & Output Files: fem.dat

v
1
2
NP
Refine
Zoom Extends
Window & Select
Exit

Figure 22. Refinement menu

The mesh refinement will duplicate the elements, so in the half that it is done there will be 4 elements per millimetre. It will be done in the extreme that deforms, usually in the bottom one, but there are cases where the tube is deformed in the upper half, which will be shown in Results section. To do the refinement, to select the region, the coordinates of the upper left corner and lower right of the region will be provided.

On the other hand, to create the upper and lower dies, the data will be provided by a text file. This file has to have the following structure:

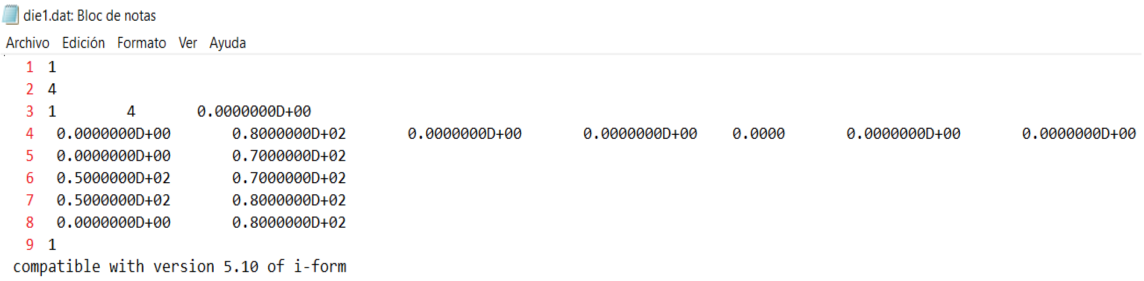

```
1 1
2 4
3 1         4       0.0000000D+00
4  0.0000000D+00       0.8000000D+02       0.0000000D+00       0.0000000D+00    0.0000       0.0000000D+00       0.0000000D+00
5  0.0000000D+00       0.7000000D+02
6  0.5000000D+02       0.7000000D+02
7  0.5000000D+02       0.8000000D+02
8  0.0000000D+00       0.8000000D+02
9 1
compatible with version 5.10 of i-form
```

Figure 23. Structure needed of the file die2.dat to load in i-Form

Line 1: 1

Line 2: number of nodes of the die

Line 3: first node / last node / 0

Line 4: coordinate X of the first node / coordinate Y of the first node / 0 / 0 / 0 / 0 / 0

Line 5: coordinate X of the second node / coordinate Y of the second node

Line 6: coordinate X of the third node / coordinate Y of the third node

Line 7: coordinate X of the fourth node / coordinate Y of the fourth node

Line 8: coordinate X of the first node / coordinate Y of the first node

Line 9: 1

It is important that between the first and the second node of the die the Y axis is contained, to avoid errors during the solving process and that the penultimate line of the file corresponds again with the first node in order to close correctly the cycle.

This example corresponds with the upper die of all the simulations carried out. The lower die change depending on the radius of it. The only lines that change are the lines 2 and 3, where there will be more nodes. Moreover, there will be more lines to provide all nodes coordinates.

Finally, to have a better approach of the radius a Matlab file was created, attached in Annex A.

The only data the file need are:

1. n: number of nodes to divide the radius
2. r: radius to divide

When this data is provided and the file is run, a text file is opened with the coordinates of all nodes. The only thing to do is to transfer these data to a file with the same structure as the explained before.

Finally, the model is ready.

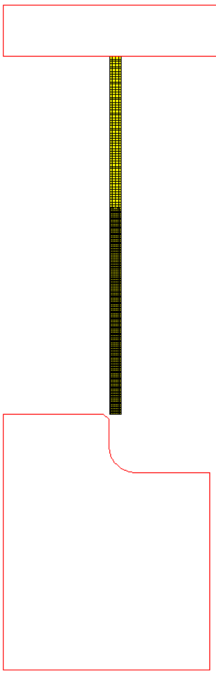

Figure 24. Final model of the process

2.2.2.2 Main Controls

In this menu, it will be defined the numbers of step to carry out during the simulation. The data needed are the starting and the target step and the increment of time between steps, which will define, along with the speed, the distance advanced in each step.

In this case the total steps will be 400.

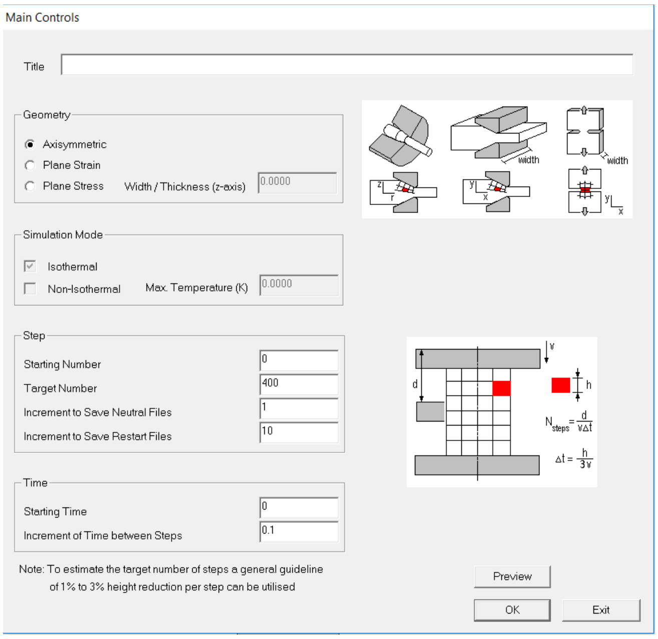

Main Controls

Title

Geometry

● Axisymmetric

○ Plane Strain

○ Plane Stress Width / Thickness (z-axis) 0.0000

Simulation Mode

☑ Isothermal

☐ Non-Isothermal Max. Temperature (K) 0.0000

Step

Starting Number 0

Target Number 400

Increment to Save Neutral Files 1

Increment to Save Restart Files 10

Time

Starting Time 0

Increment of Time between Steps 0.1

Note: To estimate the target number of steps a general guideline of 1% to 3% height reduction per step can be utilised

Figure 25. Main controls options

2.2.2.3 Dies

As is it mentioned in the section above, it is also important to define the velocity of the dies to control the distance advanced in each step. In this simulation the only die which moves is the upper one, while the other remains fixed.

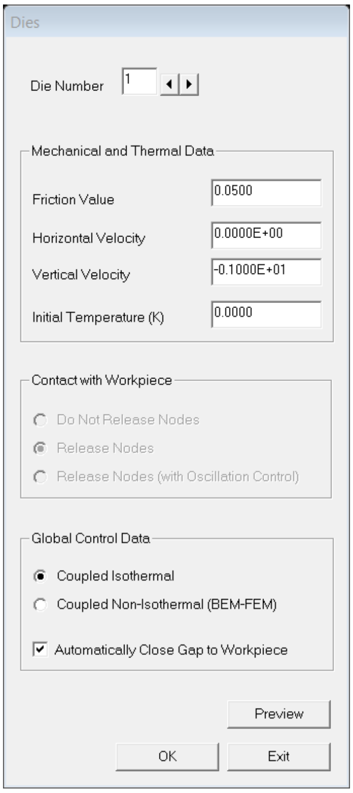

Dies

Die Number 1

Mechanical and Thermal Data

Friction Value 0.0500

Horizontal Velocity 0.0000E+00

Vertical Velocity -0.1000E+01

Initial Temperature (K) 0.0000

Contact with Workpiece

○ Do Not Release Nodes

● Release Nodes

○ Release Nodes (with Oscillation Control)

Global Control Data

● Coupled Isothermal

○ Coupled Non-Isothermal (BEM-FEM)

☑ Automatically Close Gap to Workpiece

Figure 26. Dies options

During the modelling, the first die defined was the upper one, so it will be the Die Number 1.

A friction value of m=0.05 will be introduced to simulate the effect of the lubricant used during the experimentation.

To end, the velocity of the simulation will be 1mm/step.

2.2.2.4 Material Data and Yield Criteria

Next thing to do is to define the properties of the material. As it happened for the modelling, there are two options: introducing the material by fulfilling the different gaps in the menu or by loading a database with all the information.

In this case, the chosen option was to load a database. In *"Material Database"*, it has to be selected the *"User Defined Aluminium 6xxx"* option due to during the experimentation the material was Aluminium 6063-T6.

Finally, in the bottom table (*"User Defined Material"*), it has to be ticked the Tabulated Data option. Later, the data has to be loaded by pushing *">Input Data"* and, at last, pushing *"Save Material"* in the upper-right corner.

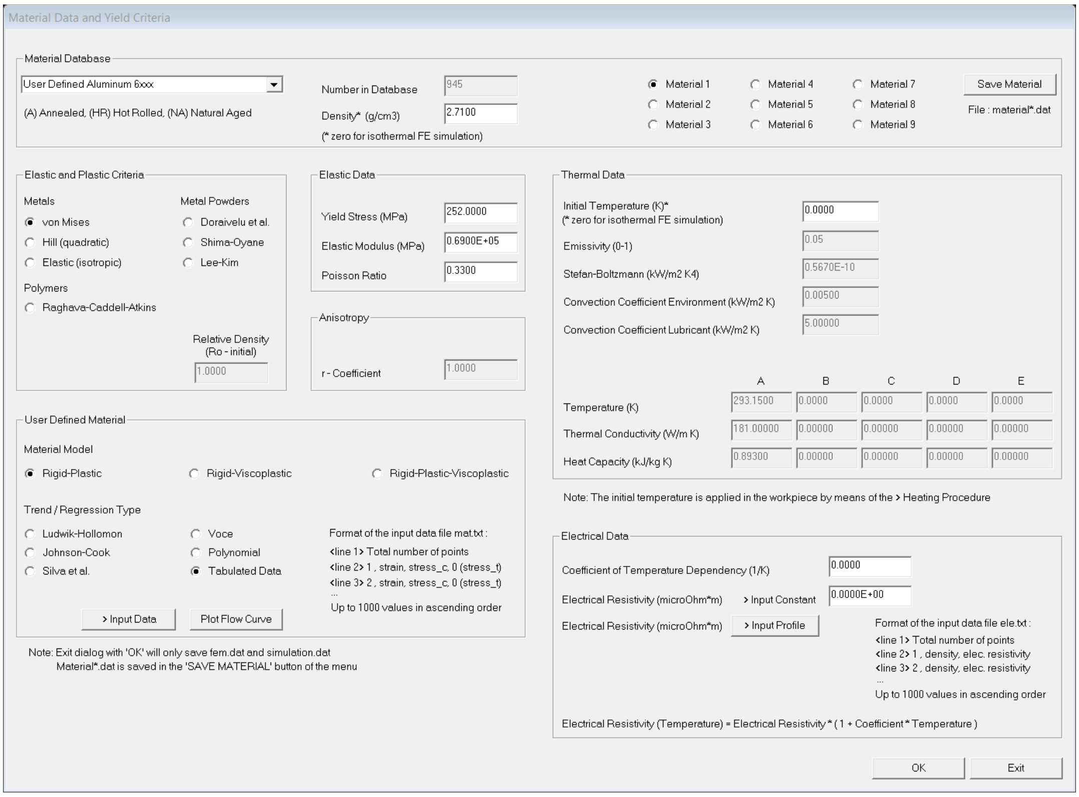
Material Data and Yield Criteria

Material Database
User Defined Aluminum 6xxx
(A) Annealed, (HR) Hot Rolled, (NA) Natural Aged
Number in Database: 945
Density* (g/cm3): 2.7100
(* zero for isothermal FE simulation)
● Material 1 ○ Material 2 ○ Material 3 ○ Material 4 ○ Material 5 ○ Material 6 ○ Material 7 ○ Material 8 ○ Material 9
File : material*.dat

Elastic and Plastic Criteria
Metals: ● von Mises ○ Hill (quadratic) ○ Elastic (isotropic)
Metal Powders: ○ Doraivelu et al. ○ Shima-Oyane ○ Lee-Kim
Polymers: ○ Raghava-Caddell-Atkins
Relative Density (Ro - initial): 1.0000

Elastic Data
Yield Stress (MPa): 252.0000
Elastic Modulus (MPa): 0.6900E+05
Poisson Ratio: 0.3300

Anisotropy
r - Coefficient: 1.0000

Thermal Data
Initial Temperature (K)*: 0.0000
(* zero for isothermal FE simulation)
Emissivity (0-1): 0.05
Stefan-Boltzmann (kW/m2 K4): 0.5670E-10
Convection Coefficient Environment (kW/m2 K): 0.00500
Convection Coefficient Lubricant (kW/m2 K): 5.00000

	A	B	C	D	E
Temperature (K)	293.1500	0.0000	0.0000	0.0000	0.0000
Thermal Conductivity (W/m K)	181.00000	0.00000	0.00000	0.00000	0.00000
Heat Capacity (kJ/kg K)	0.89300	0.00000	0.00000	0.00000	0.00000

Note: The initial temperature is applied in the workpiece by means of the > Heating Procedure

User Defined Material
Material Model: ● Rigid-Plastic ○ Rigid-Viscoplastic ○ Rigid-Plastic-Viscoplastic
Trend / Regression Type: ○ Ludwik-Hollomon ○ Johnson-Cook ○ Silva et al. ○ Voce ○ Polynomial ● Tabulated Data

Format of the input data file mat.txt :
<line 1> Total number of points
<line 2> 1 , strain, stress_c, 0 (stress_t)
<line 3> 2 , strain, stress_c, 0 (stress_t)
...
Up to 1000 values in ascending order

Note: Exit dialog with 'OK' will only save fem.dat and simulation.dat
Material*.dat is saved in the 'SAVE MATERIAL' button of the menu

Electrical Data
Coefficient of Temperature Dependency (1/K): 0.0000
Electrical Resistivity (microOhm*m) > Input Constant: 0.0000E+00
Electrical Resistivity (microOhm*m)

Format of the input data file ele.txt :
<line 1> Total number of points
<line 2> 1 , density, elec. resistivity
<line 3> 2 , density, elec. resistivity
...
Up to 1000 values in ascending order

Electrical Resistivity (Temperature) = Electrical Resistivity * (1 + Coefficient * Temperature)

Figure 27. Material Data and Yield Criteria

Once the material has been saved, the next thing is to assign the material to the workpiece. To do this, and remembering that there is only one piece, the material will be assigned by pushing *“Assign All”*.

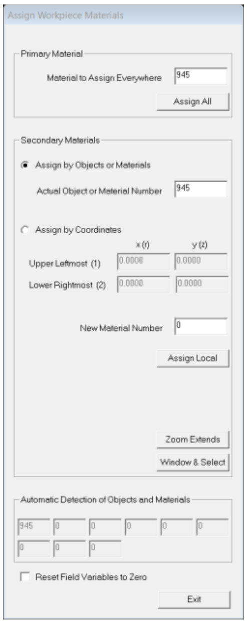

Assign Workpiece Materials

Primary Material

Material to Assign Everywhere: 945

Secondary Materials

● Assign by Objects or Materials

Actual Object or Material Number: 945

○ Assign by Coordinates

	x (r)	y (z)
Upper Leftmost (1)	0.0000	0.0000
Lower Rightmost (2)	0.0000	0.0000

New Material Number: 0

Automatic Detection of Objects and Materials

945 0 0 0 0 0
0 0 0

☐ Reset Field Variables to Zero

Figure 28. Assigning material options

2.2.2.5 Damage and Fracture controls

It is time now to define the damage model and taking into account the different analysis that will be studied, the selected one is *“McClintock – Stress Triaxiality”* which will allow to study the critical damaged in the different cases.

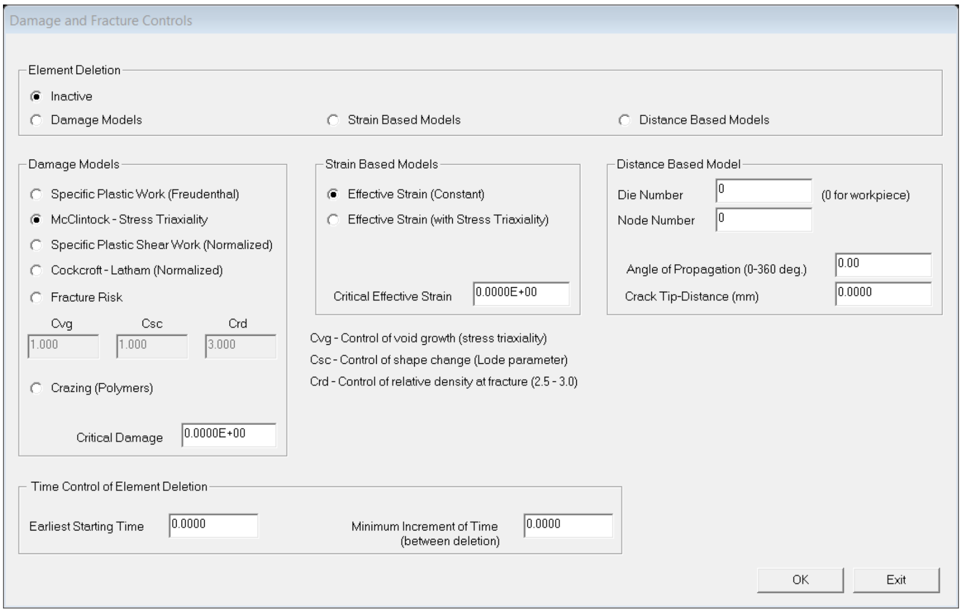

Damage and Fracture Controls

Element Deletion

● Inactive
○ Damage Models
○ Strain Based Models
○ Distance Based Models

Damage Models

○ Specific Plastic Work (Freudenthal)
● McClintock - Stress Triaxiality
○ Specific Plastic Shear Work (Normalized)
○ Cockcroft - Latham (Normalized)
○ Fracture Risk

Cvg	Csc	Crd
1.000	1.000	3.000

○ Crazing (Polymers)

Critical Damage: 0.0000E+00

Strain Based Models

● Effective Strain (Constant)
○ Effective Strain (with Stress Triaxiality)

Critical Effective Strain: 0.0000E+00

Cvg - Control of void growth (stress triaxiality)
Csc - Control of shape change (Lode parameter)
Crd - Control of relative density at fracture (2.5 - 3.0)

Distance Based Model

Die Number: 0 (0 for workpiece)
Node Number: 0

Angle of Propagation (0-360 deg.): 0.00
Crack Tip-Distance (mm): 0.0000

Time Control of Element Deletion

Earliest Starting Time: 0.0000
Minimum Increment of Time (between deletion): 0.0000

Figure 29. Damage and Fracture controls

2.2.3 Simulation process

To carry out the simulation, it will be opened now the I-form 2D program. Once it is opened the windows command screen appears.

All the necessary to perform it is to specified the root of the folder containing all the data defined in the pre-processor. It is only necessary that this data is in a folder named Run2d contained in the root of the hard disk (C:\Run2d\...). For instance:

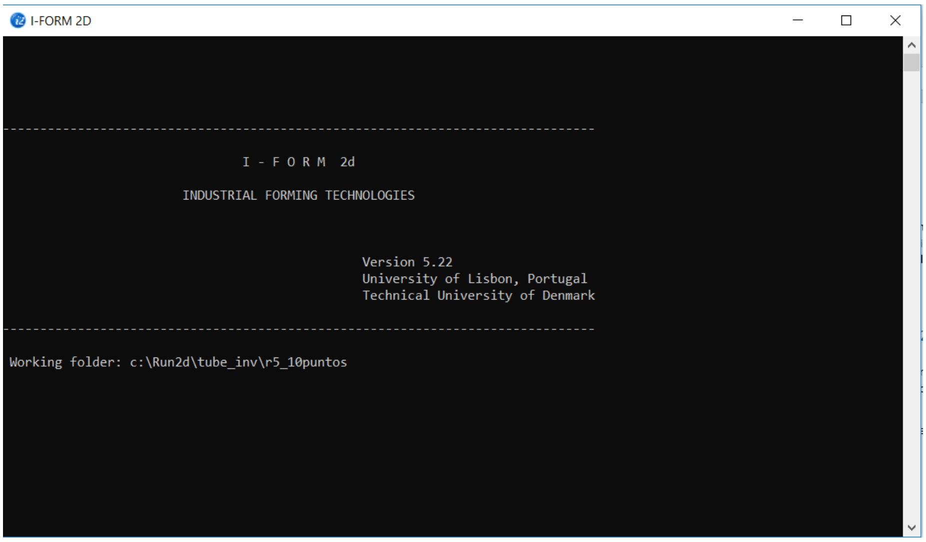

```
-------------------------------------------------------------------------------

                              I - F O R M  2d

                       INDUSTRIAL  FORMING  TECHNOLOGIES


                                               Version 5.22
                                               University of Lisbon, Portugal
                                               Technical University of Denmark

-------------------------------------------------------------------------------

 Working folder: c:\Run2d\tube_inv\r5_10puntos
```

Figure 30. Initial simulation window

When you press “Enter”, if everything is alright, everything defined previously will appear as “Active”:

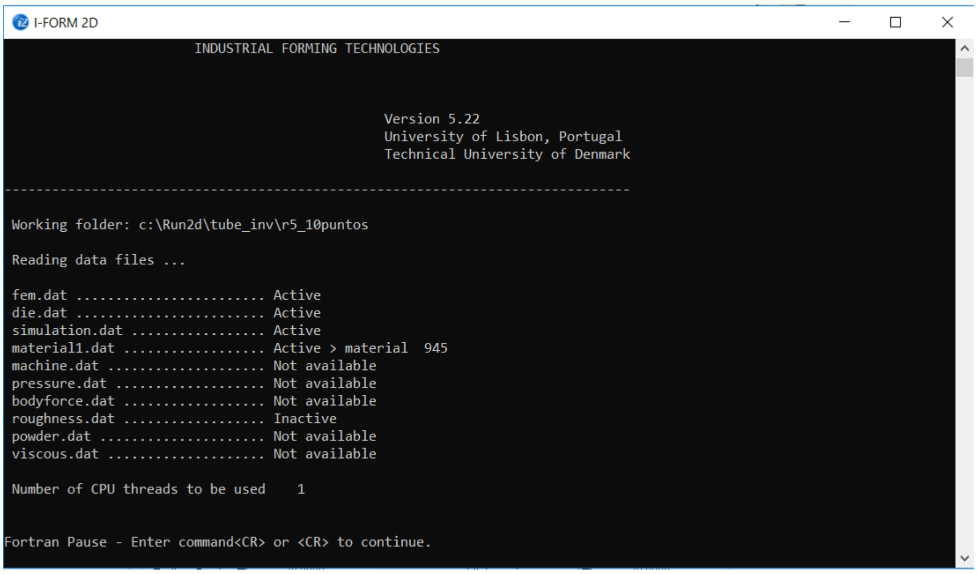

```
                        INDUSTRIAL  FORMING  TECHNOLOGIES


                                                Version 5.22
                                                University of Lisbon, Portugal
                                                Technical University of Denmark

-------------------------------------------------------------------------------

 Working folder: c:\Run2d\tube_inv\r5_10puntos

 Reading data files ...

 fem.dat ........................ Active
 die.dat ........................ Active
 simulation.dat ................. Active
 material1.dat .................. Active > material  945
 machine.dat .................... Not available
 pressure.dat ................... Not available
 bodyforce.dat .................. Not available
 roughness.dat .................. Inactive
 powder.dat ..................... Not available
 viscous.dat .................... Not available

 Number of CPU threads to be used    1


Fortran Pause - Enter command<CR> or <CR> to continue.
```

Figure 31. Ready simulation window for the process

Finally, by pressing “Enter” again, the simulation will be carried out.

2.2.4 Postprocessor

As soon as the simulation has finished, it is possible to analyse a huge quantity of variables, such as surface strains, velocity, force, stress, ductile damage…

This project it is focused in analysing the evolution of the force, the surface strain, the ductile damage and the stress triaxiality, therefore, it will be explained how to extract these results.

2.2.4.1 Forces

One of the main purposes of this document is to show how the forces vary depending on the tube's radius.

Getting this information is easy. The methodology to follow is:

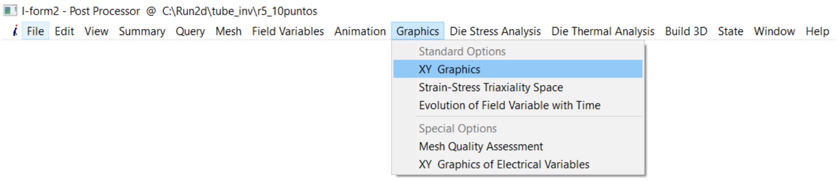
I-form2 - Post Processor @ C:\Run2d\tube_inv\r5_10puntos
File
Edit
View
Summary
Query
Mesh
Field Variables
Animation
Graphics
Die Stress Analysis
Die Thermal Analysis
Build 3D
State
Window
Help
Standard Options
XY Graphics
Strain-Stress Triaxiality Space
Evolution of Field Variable with Time
Special Options
Mesh Quality Assessment
XY Graphics of Electrical Variables

Figure 32. Selection of the different graphics types

When the XY Graphics menu is opened there are several options:

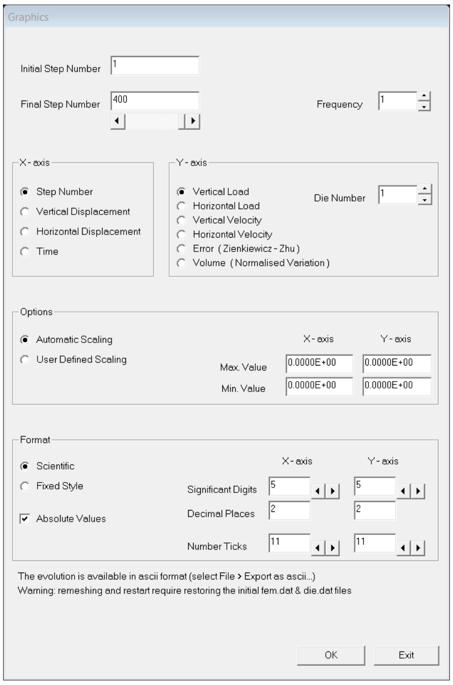

Initial Step Number: 1
Final Step Number: 400
Frequency: 1

X - axis
● Step Number
○ Vertical Displacement
○ Horizontal Displacement
○ Time

Y - axis
● Vertical Load
○ Horizontal Load
○ Vertical Velocity
○ Horizontal Velocity
○ Error (Zienkiewicz - Zhu)
○ Volume (Normalised Variation)
Die Number: 1

Options
● Automatic Scaling
○ User Defined Scaling

	X - axis	Y - axis
Max. Value	0.0000E+00	0.0000E+00
Min. Value	0.0000E+00	0.0000E+00

Format
● Scientific
○ Fixed Style
☑ Absolute Values

	X - axis	Y - axis
Significant Digits	5	5
Decimal Places	2	2
Number Ticks	11	11

The evolution is available in ascii format (select File > Export as ascii...)
Warning: remeshing and restart require restoring the initial fem.dat & die.dat files

Figure 33. XY Graphics options

In this case, the required information is the step number (later is immediate to change the step into vertical displacement) in the X axis and the vertical load in the Y axis. When those options are marked, it is possible to export an asci file with the data as follows:

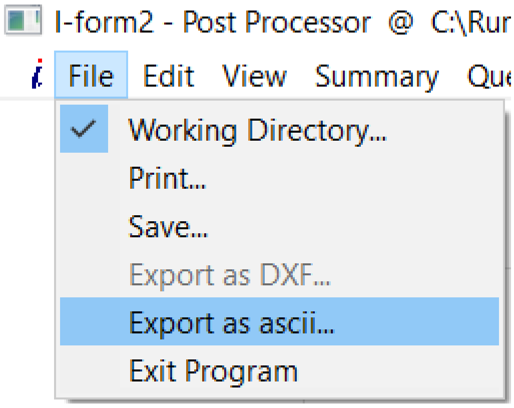
I-form2 - Post Processor @ C:\Rur
File
Edit
View
Summary
Que
Working Directory...
Print...
Save...
Export as DXF...
Export as ascii...
Exit Program

Figure 34. How to export the information

The data will be export in a text file in the working directory with the name *"fem.asc"*, which can be easily copied to an excel file.

2.2.4.2 Surface Strain

During the analytical experimentation, the external surface of the tube was painted in white and later sprayed with black droplets, generating a non-uniform speckle pattern, in order to use de digital image correlation (DIC).

In this case, using the numerical model it is more immediate to get these results:

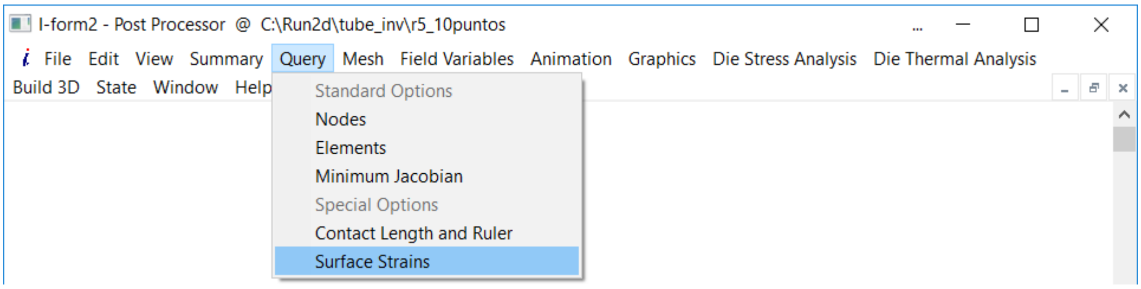
I-form2 - Post Processor @ C:\Run2d\tube_inv\r5_10puntos
File
Edit
View
Summary
Query
Mesh
Field Variables
Animation
Graphics
Die Stress Analysis
Die Thermal Analysis
Build 3D
State
Window
Help
Standard Options
Nodes
Elements
Minimum Jacobian
Special Options
Contact Length and Ruler
Surface Strains

Figure 35. How to access to the surface strains

Later, the following menu appears:

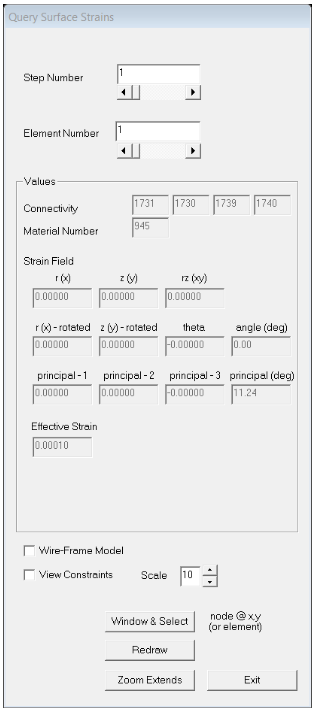
Query Surface Strains
Values
Strain Field
☐ Wire-Frame Model
☐ View Constraints
Window & Select
node @ x,y (or element)
Redraw
Zoom Extends
Exit

Step Number: 1
Element Number: 1
Connectivity: 1731 1730 1739 1740
Material Number: 945
r (x): 0.00000
z (y): 0.00000
rz (xy): 0.00000
r (x) - rotated: 0.00000
z (y) - rotated: 0.00000
theta: -0.00000
angle (deg): 0.00
principal - 1: 0.00000
principal - 2: 0.00000
principal - 3: -0.00000
principal (deg): 11.24
Effective Strain: 0.00010
Scale: 10

Figure 36. Surface strains menu

Here, it can be selected the step number to extract the strain and the desired element. It can be extracted the global strains, local strains and principal strains of it.

2.2.4.3 Ductile damage

Another analysis to be done is to establish ductile damage criteria for the tube inversion. For this reason, it is important to know how the damage varies and where it is concentrated.

To extract this information, there is a simple option:

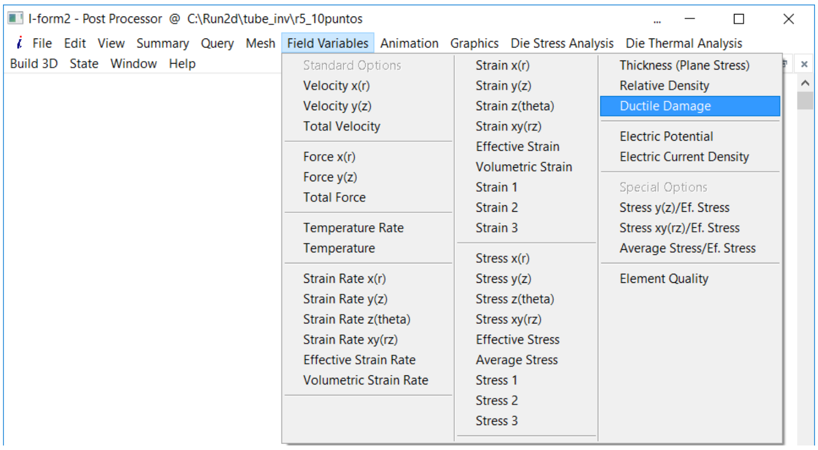
I-form2 - Post Processor @ C:\Run2d\tube_inv\r5_10puntos
File Edit View Summary Query Mesh Field Variables Animation Graphics Die Stress Analysis Die Thermal Analysis
Build 3D State Window Help
Standard Options
Velocity x(r)
Velocity y(z)
Total Velocity
Force x(r)
Force y(z)
Total Force
Temperature Rate
Temperature
Strain Rate x(r)
Strain Rate y(z)
Strain Rate z(theta)
Strain Rate xy(rz)
Effective Strain Rate
Volumetric Strain Rate
Strain x(r)
Strain y(z)
Strain z(theta)
Strain xy(rz)
Effective Strain
Volumetric Strain
Strain 1
Strain 2
Strain 3
Stress x(r)
Stress y(z)
Stress z(theta)
Stress xy(rz)
Effective Stress
Average Stress
Stress 1
Stress 2
Stress 3
Thickness (Plane Stress)
Relative Density
Ductile Damage
Electric Potential
Electric Current Density
Special Options
Stress y(z)/Ef. Stress
Stress xy(rz)/Ef. Stress
Average Stress/Ef. Stress
Element Quality

Figure 37. How to extract the ductile damage

Once the menu is opened, the most important option is the first one, to select the step number.

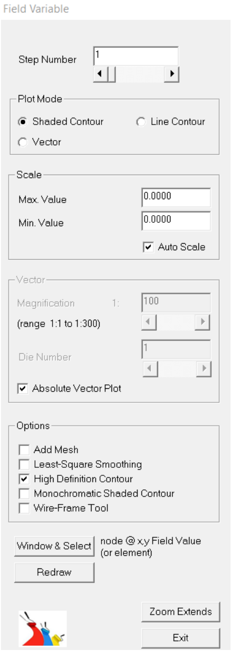

Field Variable

Step Number: 1

Plot Mode

● Shaded Contour ○ Line Contour

○ Vector

Scale

Max. Value: 0.0000

Min. Value: 0.0000

☑ Auto Scale

Vector

Magnification 1: 100

(range 1:1 to 1:300)

Die Number: 1

☑ Absolute Vector Plot

Options

☐ Add Mesh

☐ Least-Square Smoothing

☑ High Definition Contour

☐ Monochromatic Shaded Contour

☐ Wire-Frame Tool

Figure 38. Ductile damage menu

2.2.4.4 Effective strain vs stress-triaxiality

To analyse this data, the menu *Effective Strains vs. Stress Triaxiality* has to be selected in the *Graphics* option. Once it is selected the next menu appears:

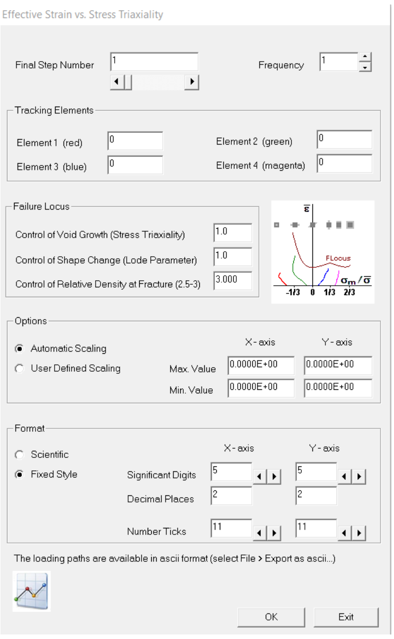

Effective Strain vs. Stress Triaxiality

Final Step Number: 1

Frequency: 1

Tracking Elements

Element 1 (red): 0

Element 2 (green): 0

Element 3 (blue): 0

Element 4 (magenta): 0

Failure Locus

Control of Void Growth (Stress Triaxiality): 1.0

Control of Shape Change (Lode Parameter): 1.0

Control of Relative Density at Fracture (2.5-3): 3.000

Options

● Automatic Scaling

○ User Defined Scaling

	X - axis	Y - axis
Max. Value	0.0000E+00	0.0000E+00
Min. Value	0.0000E+00	0.0000E+00

Format

○ Scientific

● Fixed Style

	X - axis	Y - axis
Significant Digits	5	5
Decimal Places	2	2
Number Ticks	11	11

The loading paths are available in ascii format (select File > Export as ascii...)

Figure 39. Effective Strain vs. Stress Triaxiality menu.

The fields to fulfil are the *Final Step Number* and the *Tracking Element*, which will allow to define the results to extract. As it happened for the forces, it is possible to export an asci file with the data.

3. Results

3.1 Introduction

The aim of this section is showing the different possibilities that a tube has when it comes to external inversion processes.

For this reason, results will be shown since a really small radius *(R=0.5 mm)* to a large radius *(R=20 mm)*, comparing the force evolution, the strain paths and, finally, the ductile damage that the tube is able to withstand in each case.

All these results will be also compared with experimental results obtained in previous researches, shown in the document J.P. Magrinho, M.B. Silva, & and G. Centeno et al., 2019, performed on a hydraulic testing machine (Instron SATEC 1200 kN). This will allow to validate the numerical results obtained within this work.

3.2 Force analysis

In the force analysis can be distinguished mainly three different evolutions, depending on the inversion radii. This is the reason why it will be divided in three sections.

3.2.1 Small inversion radius

To analyse the effect of small radius in the inversion process, the chosen radius was *R=0.5 mm.* In these cases, where the radius is almost non-existent, it can be observed that an instability appears, concretely local buckling at the top of the tube.

This effect also occurs in the instability process, where the tube is pushed against a plane die in order to determine the maximum force that can be applied to the tube.

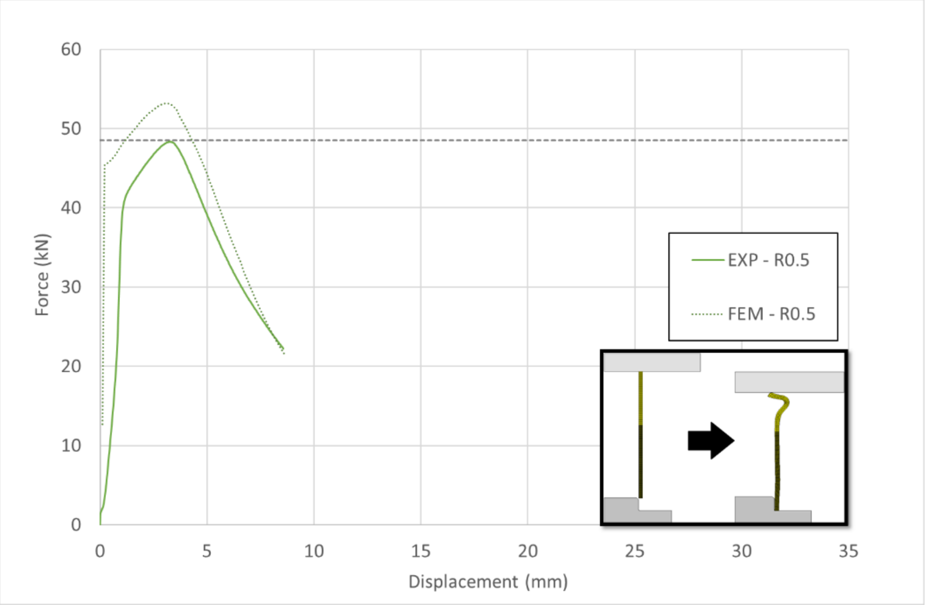

Figure 40. Evolution of the force for R=0.5 mm

As it is shown in the figure above, the force augment until it reaches its maximum, where the instability appears and it starts to decrease.

It can be appreciated that the evolution of the forces in both cases (experimental and numerical) are very similar, even the maximum value of it (although in the FEM case is bigger), making valid the results obtained by numerical model to represent what happens in the experiments carried out in the laboratory.

3.2.2 Large inversion radius

In this case it will be analysed the other extreme, corresponding with a large inversion radius, as it can be *R=20 mm*. This time, the force increases in the whole process until it reaches the failure.

Due to the radius, the tube does not invert, but adopt the shape of the bottom die and continues down the surface, provoking that the thickness decreases, starting a necking process which leads to the appearance of cracks.

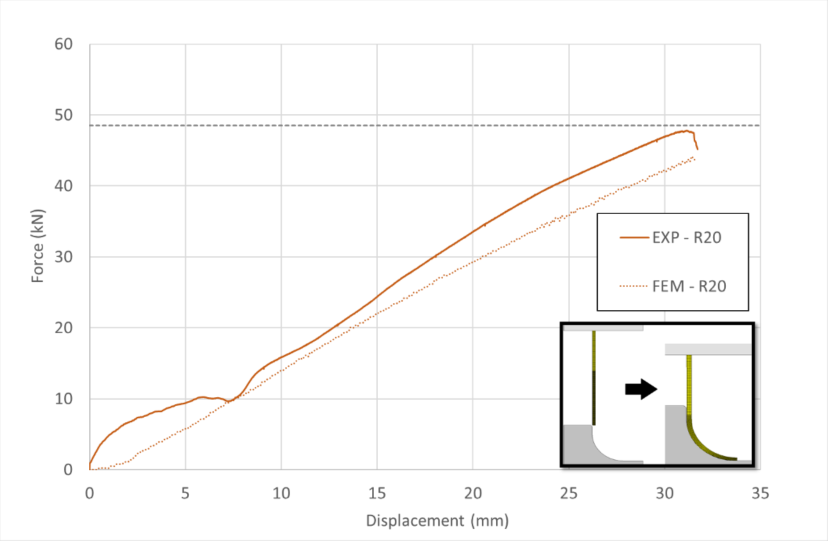

Figure 41. Evolution of the force for R=20 mm

In this figure, the simulation continues until a displacement of the upper over 30 mm, but as it will be explained in the *“Ductile damage”* section this is unreal due to the tube starts the necking process in a lower displacement.

3.2.3 Intermediate inversion radius

Finally, it will be analysed an intermediate radius such as R=5 mm, where the complete inversion of the tube takes place. The evolution of the force is shown in the figure.

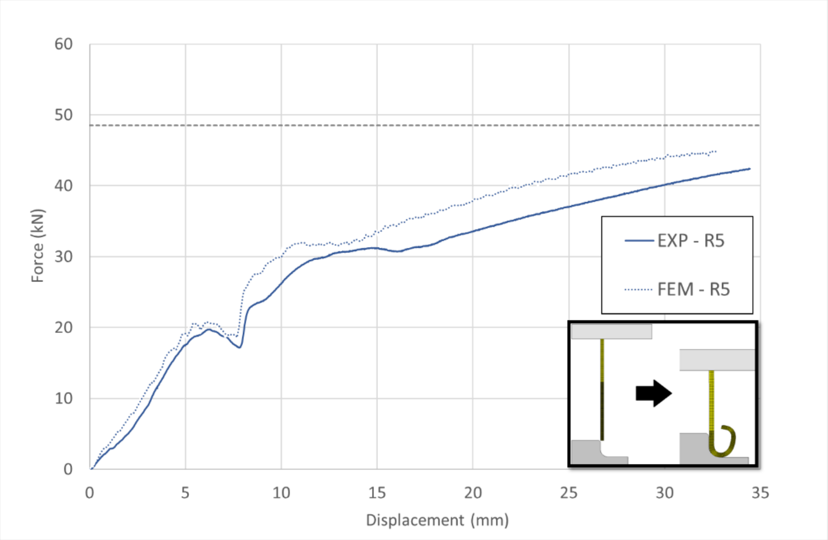

Figure 42. Evolution of the force for R=5 mm

As it can be seen, there are 3 different stages. The first one, since the tube first touches the inversion radius, where the force starts to increases, until the extreme of the tube reaches the final of the inversion. At this point, the force decreases due to the tube is adapting to the radius. Once that the tube has adopted the shape of the bottom die, the force increases again, until the inversion process is completed.

The evolution of the tube in the different stages is represented below:

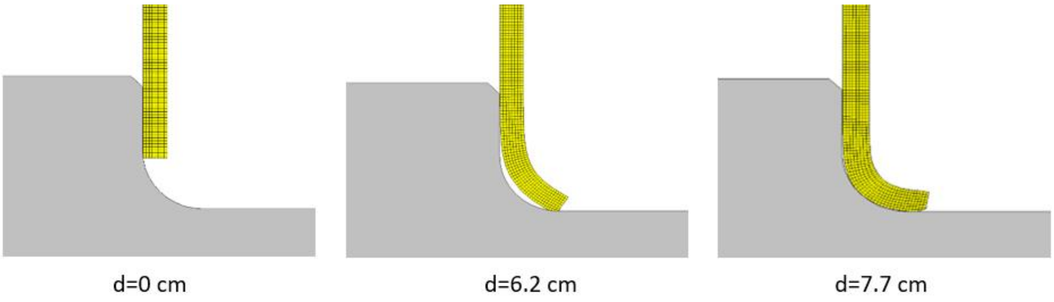

Figure 43. Different stages of the successful tube inversion

Now that the three different possibilities in an inversion process have been explained, they will be represented in the same figure.

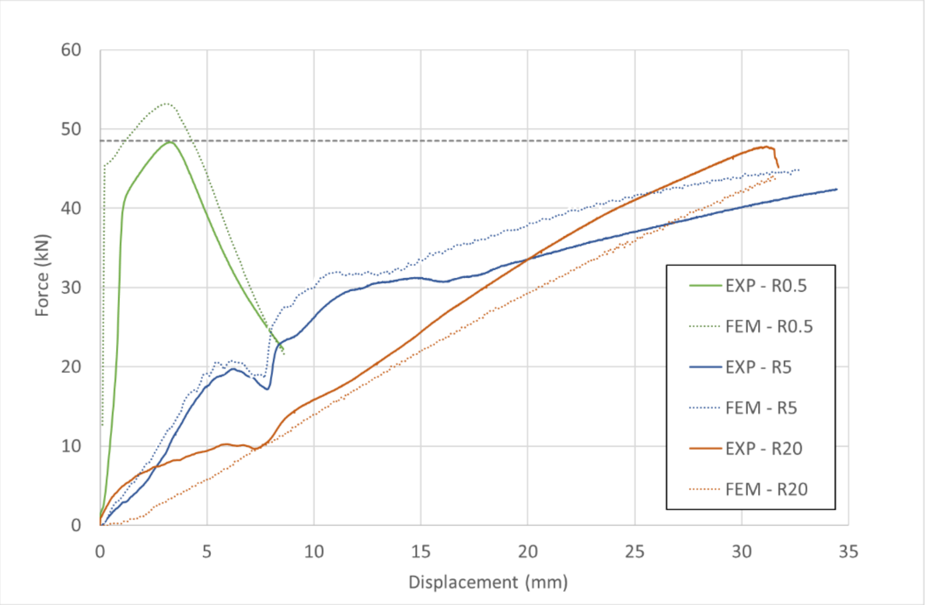

Figure 44. . Evolution of the forces

Once the evolution of the forces has been analysed for each case, it is clear that the inversion radius models the type of process that takes place. The processes are instability for small radii, complete inversion for intermediate radii and expansion for large radii.

3.3 Strain analysis

As it has been explained in Section 3.2, the inversion process varies according to the inversion radius of the bottom die. Therefore, this section will be divided into three, analysing the results independently for each case.

3.3.1 Small inversion radius

For this section the simulation will be done with R=0.5mm and the refinement of the mesh is done in the upper extreme, due to, as commented before, the instability appears here. The element that will be selected to represent the surface strains will be the *Element 1988*, which corresponds with a point located in the centre of the buckling zone, as shown in figure:

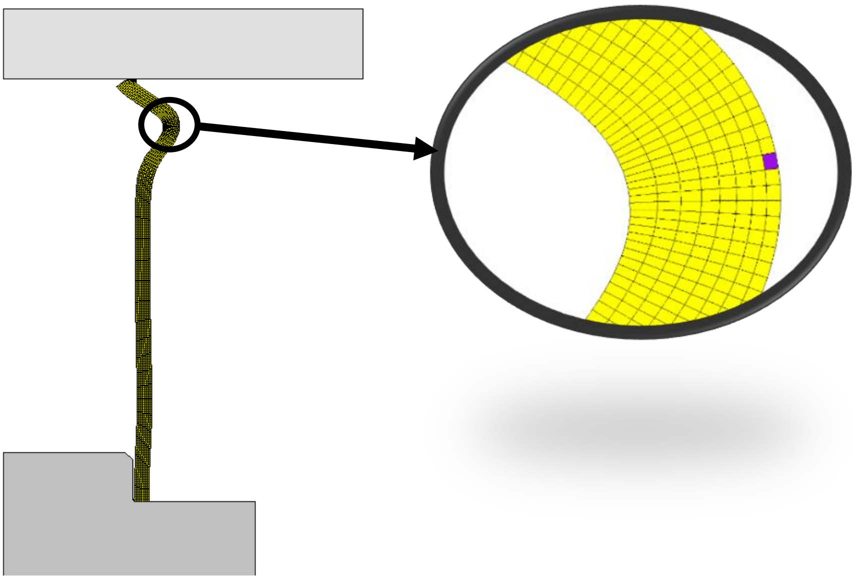

Figure 45. Final state of the tube and location of the element analysed

Representing the surface strain of this point and comparing with the results obtained in the analytical process:

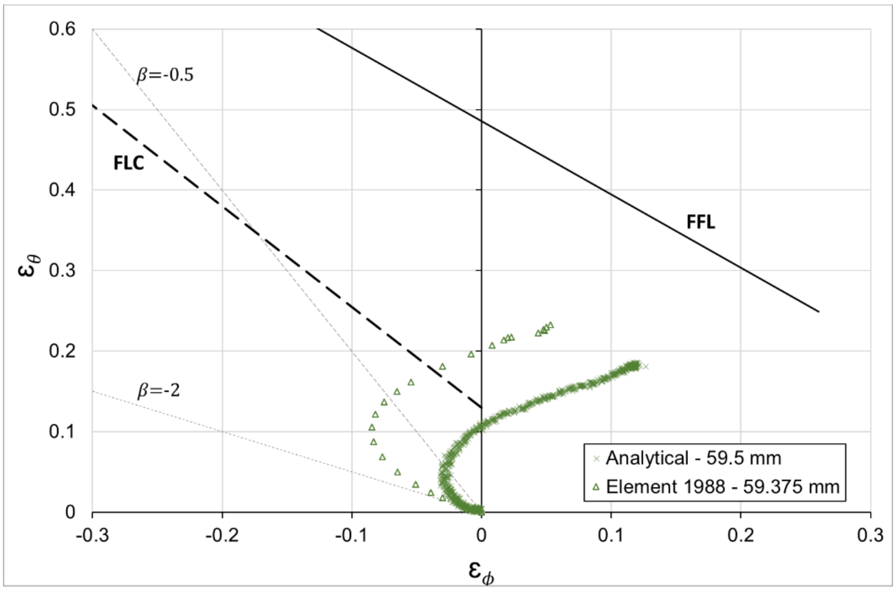

Figure 46. Strain evolution for R=0.5 mm

The strain starts with a *β=-2,* which corresponds with *Uniaxial Compression* where the tube decreases the length in that zone whereas the circumferential length augments. This entails that the thickness increase.

Although the strain values are not similar in the whole figure, the evolution that they follow are. The values only are close at the beginning of the buckling, which leads to think that there are some errors in the numerical model in terms of strain for small radii.

3.3.2 Large inversion radius

In this case, the simulation will be done with R=20 mm and the chose element is the *Element 583*, which is 0.625 mm from the lower extreme of the tube in the external tube side. Moreover, it will be analysed the *Element 575*, which corresponds with the same point, but in the initial internal side.

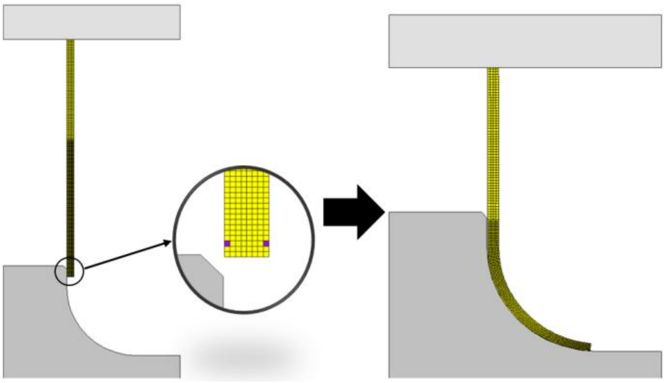

Figure 47. Location of the element analysed and final position of the tube

The evolution of the strain is:

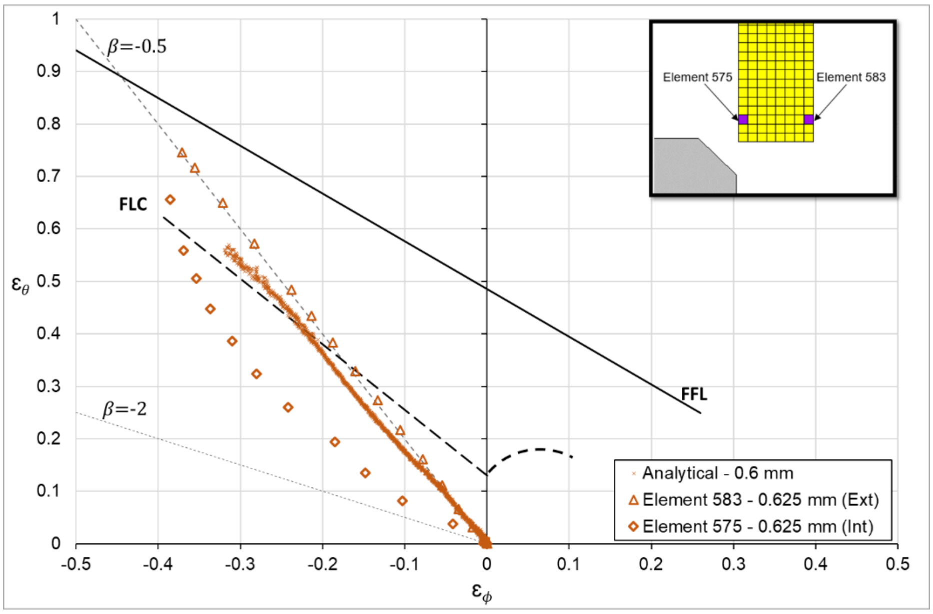

Figure 48. Strain evolution for R=20 mm

The evolution in this case is very similar in both cases, which means that the numerical model is a good approach. As it can be seen, the trajectory follows the line of β=-0.5, which corresponds with *Uniaxial tension*, meaning that the tube decreases its length while increasing its circumferential length, provoking that the thickness also decreases. Because of the decrease in the thickness, the necking process will appear which will lead to the creation of a crack.

3.3.3 Intermediate inversion radius

Finally, now it will be represented the case in which the inversion is successful, corresponding with an intermediate radius. The chosen radius to show the results is again *R= 5 mm*. In this case, it will be analysed the *Element 572*, in the external side, and the *Element 561*, in the internal side of the tube.

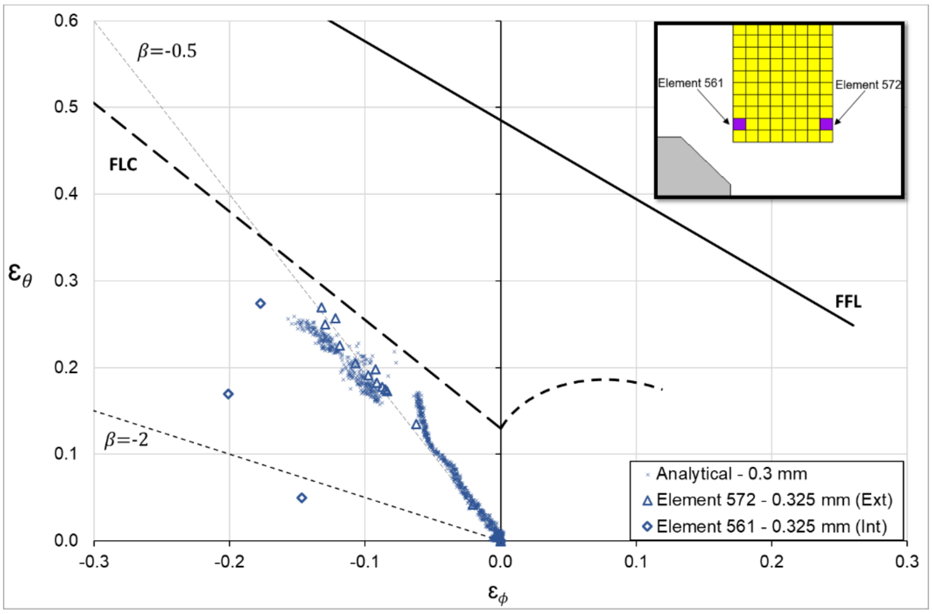

Figure 49. Strain evolution for R=5 mm

This figure depicts the strain path for the successful inversion process. As it happened for the large radius, the trajectory that follows is *β=-0.5,* corresponding with *Uniaxial tension,* with the difference that in this case the absolute values of the strains grow until the inversion is completed in that point. Later, the strains values decrease and remains constant. In the next table, the values of the strains are presented:

Displacement of the upper die	ε_θ	ε_ϕ
0	-0.00006	0.00011
2.5	-0.02077	0.0419
5	-0.06227	0.13474
7.5	-0.09234	0.19824
10	-0.12198	0.25703
12.5	-0.13226	0.26928
15	-0.12941	0.25005
17.5	-0.11873	0.22508
20	-0.10711	0.2048
22.5	-0.09771	0.19093
25	-0.09131	0.18245
27.5	-0.08741	0.1776
30	-0.08519	0.17485
32.5	-0.08388	0.17311

Table 2. Strain values for different displacements of the upper die

Once the three possibilities for inversion has been defined, it is the time to define which are the ranges of radii for a successful inversion. At one extreme, the failure is provoked by local buckling at the top extreme of the tube; at the other, the excessive decrease of the thickness favours the appearance of a crack.

After carrying out some simulations more for small radius (from 0.5 mm to 5 mm), the results reached are:

Inversion radius of the lower die (mm)						
0.5	0.6	0.8	1	2	3	5
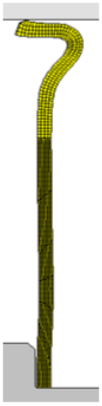	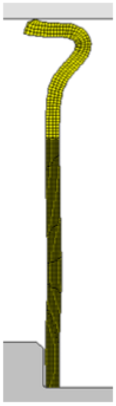	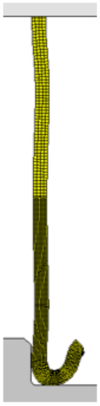	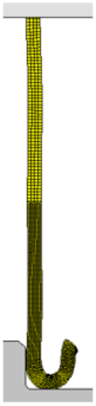	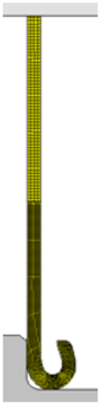	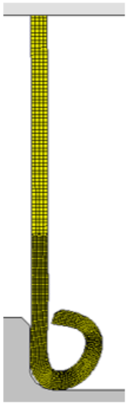	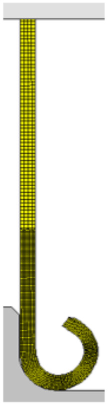
Displacement of the upper die (mm)						
20	20	20	20	20	30	30
Local buckling	Local buckling	Partial inversion	Partial inversion	Partial inversion	Inversion	Inversion

Figure 50. Final state of the tube for each small inversion radius

As it is shown in the table, for inversion radii smaller than *R=0.8 mm*, there is directly local buckling at the top of the tube, while for radii equal or larger than R=0.8 *mm* to *R=3 mm*, there is a partly inversion. In the table are indicated the maximum displacement of the upper die without the appearance of instabilities.

For *R=3 mm* or larger, the potential mode of failure is that the tube may end up bumping against itself, causing an instability in the top of the tube. For example, if the simulation for *R=3 mm* continues until an upper displacement of 40 mm, the result will be the following:

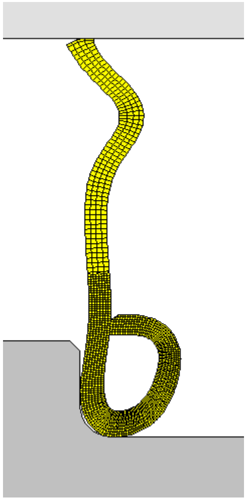

Figure 51. Example of mode of failure for R=3 mm

On the other hand, if the radius is larger than 5 mm, the results are these:

Inversion radius of the lower die (mm)								
5	6	7	8	9	10	11	12	15
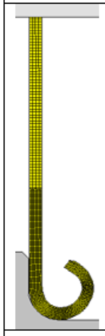	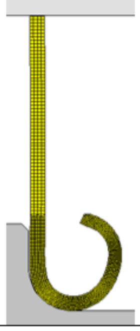	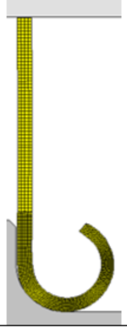	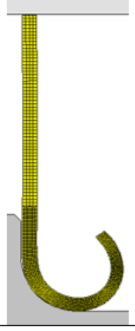	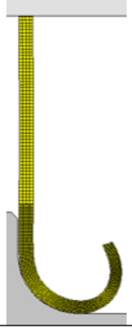	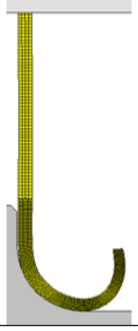	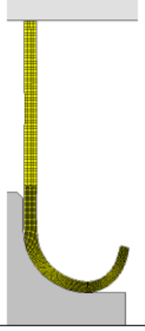	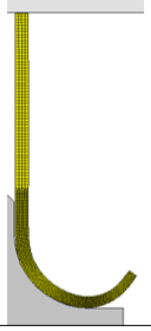	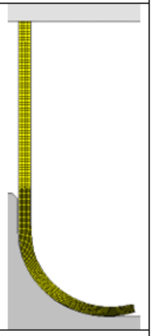
Displacement of the upper die (mm)								
30	40	40	40	40	40	40	40	40
Inversion	Inversion	Inversion	Inversion	Inversion	Inversion	Inversion	Inversion	Necking

*It is not clear if the tube can invert without taking into account the ductile damage

Figure 52.Final state of the tube for large inversion radius

The table depicts the state of the tube at the end of the simulation and as it can be seen, there is a successful inversion for the range of radius between *R=5* and *15 mm*. For larger radius, these are so large that the tube cannot invert, but adopt the shape of the die as in the inversion process.

Next step is analysing the ductile damage in each case because, although in the simulation the result is satisfactory in terms of final shape, this may not happen in a laboratory.

3.4 Ductile damage analysis

In this section, it will be only analysed the ductile damage for large inversion radii, due to the results obtained in the previous chapters.

The critical value for the ductile damage obtained for expansion in previous researches was around *0.15*. During the inversion process with a *5 mm* radius die, the ductile damage accumulated at the end of process is bigger than that value. However, when the tube begins the inversion process, the ductile damage is lower and the process is carried out successfully.

Having this in mind, the critical ductile damage for expansion will be used for inversion as the critical damage until the moment the tube separates from the die.

Therefore, it will be considered that once the inversion process has started, it is easier for the tube to complete the inversion process rather than starting the necking process.

The beginning of the inversion will be considered the moment that the internal face of the tube separates from the die, as it is shown in the figure:

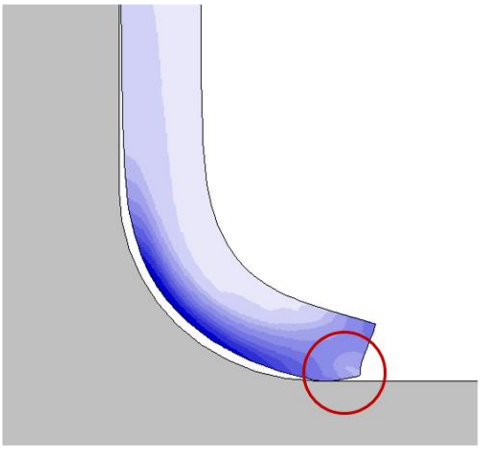

Figure 53. Moment in which the tube starts to invert

The next table shows the displacement of the upper die at the beginning of the tube inversion and the ductile damage at that moment for different inversion radii:

Inversion radius	Displacement of the upper die at the beginning of inversion (mm)	Ductile damage
5	14.5	0.1353
6	16	0.1368
7	17.5	0.1346
8	19.5	0.1394
9	20	0.1322
10	21.5	0.1359
11	24.5	0.1504
12	26.5	0.1595

Table 3. Displacement of the upper die at the beginning of the inversion and the ductile damage for each inversion radius

As table shows, the ductile damage is lower than the critical value in each case except for *R=11 and 12 mm*, so it can be concluded that the inversion is successful until an inversion *R=10 mm*. All the figures showing the ductile damage in the moment corresponding with the beginning of the inversion value are attached in the Annex B – Ductile damage.

If the inversion radius is larger than *R=10 mm*, the ductile damage surpasses the critical value, generating a crack and making the process unsuccessful.

3.5 Formability limits

The objective of this chapter is to determine the limits for a successful inversion process analysing the ductile damage (previously analysed) and the surface strains.

As it was proved in the section 3.4**Error! Reference source not found.**, in terms of ductile damage, it is not known if the process is satisfactory from *R=8 mm* and larger due to the critical value for the damage is it not clearly define for the inversion process. This is why the strain paths for *R=8 mm* and larger will be represented in the FLD.

In each case, the element analysed will be *Element 596*. The choice of this element is due to the fact that strains are concentrated in this extreme and where the FLC and FFL were calibrated in previous researches, as explained in 1.1. It will be also represented the *Element 586*, at the same distance but in the internal side of the tube.

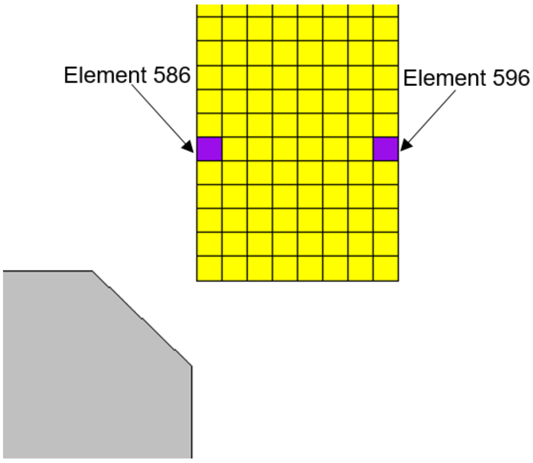

Figure 54. Elements analysed

In the next figure, it will be represented the strains since *R=8 mm* until the radius in which the FLC is clearly surpassed. The figure only shows the evolution since the beginning of the process until the moment the tube starts to invert, corresponding with the upper displacement shown in Table 3. Displacement of the upper die at the beginning of the inversion and the ductile damage for each inversion radius.

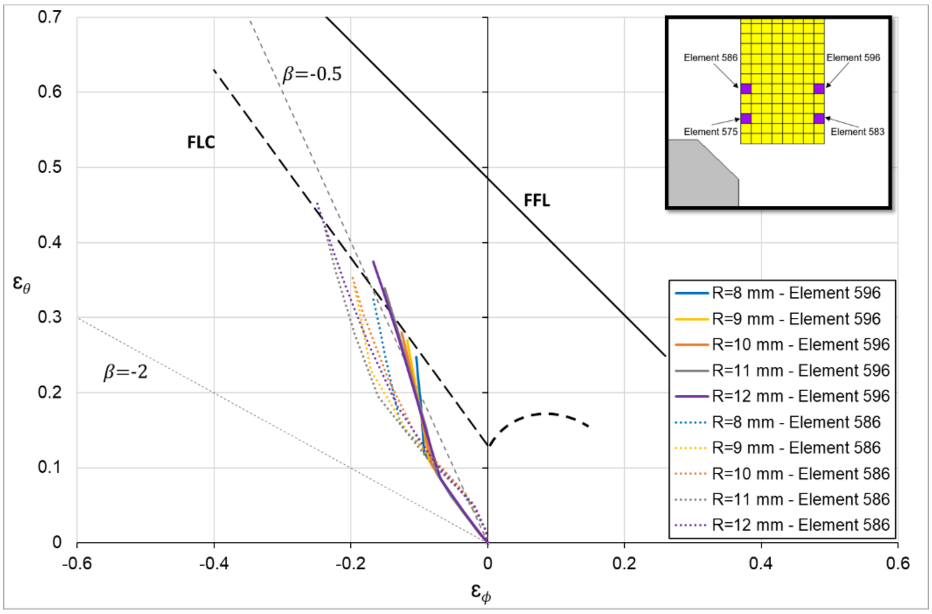

Figure 55. Strain paths

Looking in the FLD, it can be appreciated that there is no point beyond the FLC for radii smaller than *R=10 mm,* which means that the inversion process is carried out successfully.

Analysing now what happens with the *R=11 mm* case, there are some points which are above the FLC, so it is not clearly determined if the process can be carried out successfully or not. Finally, the *R=12 mm* case have many points above the FLC.

On the other hand, the strains in the internal tube side are larger than in the external one, but it happens the same as before: there is no point beyond the FLC for radii smaller than *R=10 mm.*

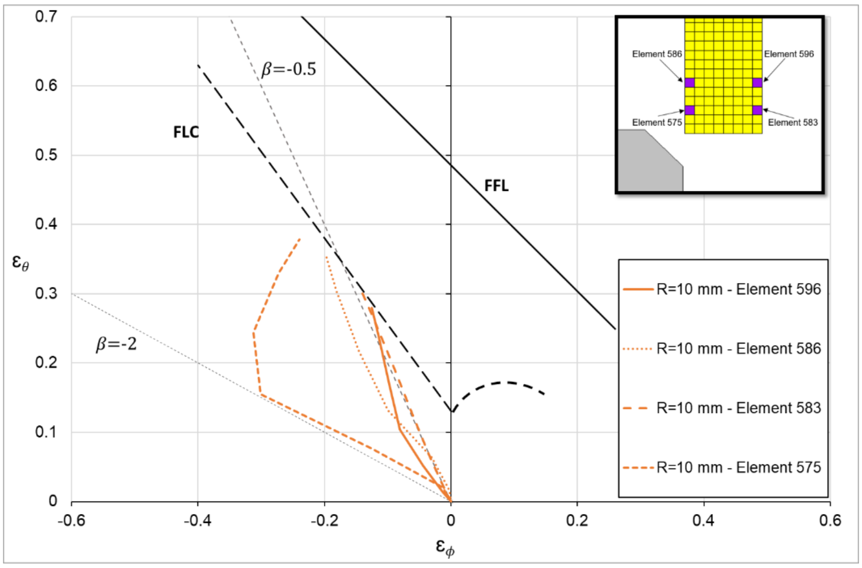

Figure 56. FLD for R=10 mm

Finally, it will be analysed the FLD for *R=10 mm*, for the elements shown in the Figure 56, to see if the choice of the element analysed affects to the final conclusion. As it is represented, the strains are bigger in the *Element 583* and *575*, but they are still below the FLC, so the conclusion will be the same.

Looking to all these data (ductile damage, strain paths and state of the inversion), it can be concluded that the inversion process is completed successfully until *R=10 mm* in the cases of *R>5 mm*. The *R=11 mm* case is not clear, but taking the results obtained it will probably have a crack.

Inversion radius	Displacement of the upper die at the beginning of inversion (mm)	ε_θ	ε_ϕ	Ductile damage	Fracture
5	14.5	-	-	0.1353	No
6	16	-0.07979	0.17197	0.1368	No
7	17.5	-0.09039	0.20369	0.1346	No
8	19.5	-0.10424	0.24756	0.1394	No
9	20.8	-0.11752	0.26983	0.1322	No
10	21.5	-0.12552	0.28012	0.1359	No
11	24.5	-0.15034	0.33943	0.1504	?
12	26.5	-0.16691	0.37469	0.1595	Yes

Table 4. Summary of the main results for each case in Element 596.

3.6 Triaxiality analysis

In this chapter, it will be represented the effective strain vs stress-triaxiality for the limit cases in large radii, corresponding with *R=9, 10* and *11 mm* for the elements previously used: *Element 596 (external tube side)* and *586 (internal tube side).*

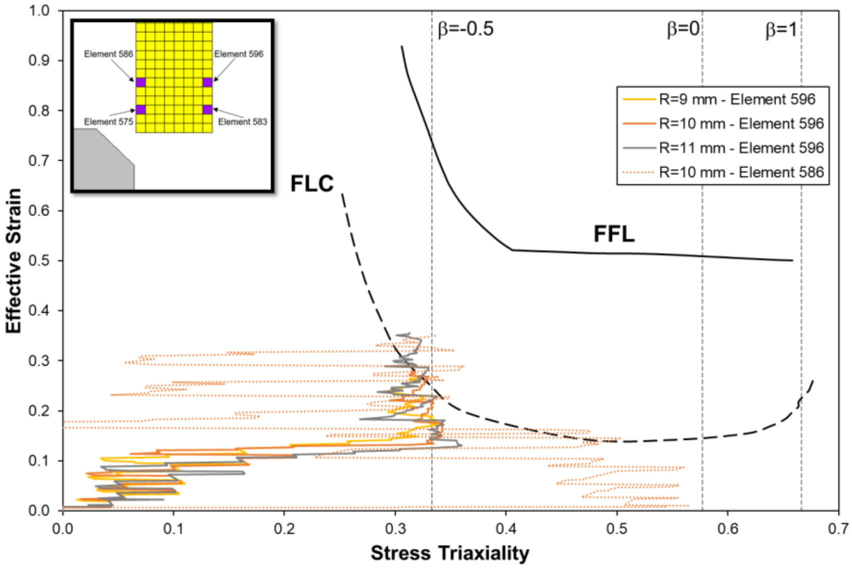

Figure 57. Space of effective strain vs stress-triaxiality

As it happened before, there are no points beyond the FLC for the cases *R<10 mm* in the *Element 596,* but there are for *R=11 mm.* This reinforces the idea that the tube will have a crack for *R=11 mm.*

Moreover, if *Element 586* (internal side) is analysed, there are a lot of points beyond the FLC. This leads to the idea that the FLC is defined conservatively and, maybe, if it is recalculated, the *R=11 mm* case is also below it.

Inversion radius of the lower die (mm)				
0.5	0.8	3	10	12
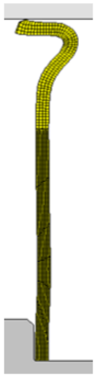	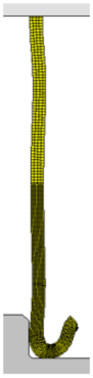	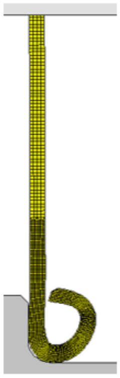	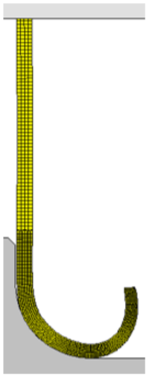	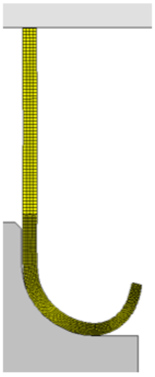
Displacement of the upper die (mm)				
20	20	20	20	40
Local buckling	Partial inversion	Inversion	Inversion	Necking

Figure 58. Limit cases

4. Conclusions and future work

In this work, it has been carried out a numerical analysis using the i-Form software for the inversion process for Aluminium AA6063-T6 tubes. The results obtained have been validated with experimental researches made before for inversion processes with radii 0.5, 5 and 20 mm of the die.

Once all the results - divided in four different categories: forces, surface strain, ductile damage and triaxiality - have been analysed and the conclusions reached are:

- The assumptions taken from sheet metal forming are valid for tube forming.
- The evolution of the forces obtained in i-Form are very close to the experimental ones, making possible to predict this evolution for the different inversion cases.
- In terms of surface strains, the results obtained are very good when the inversion takes place. However, for small inversion radii, although the evolution has the same trajectory, the values of the strains differs substantially.
- During the inversion process the trajectory of the strains for a point at the lower extreme of the tube follows the $\beta=-0.5$ line, which means *Uniaxial tension.* This also happened during the expansion process.
- It has been demonstrated that the forming limits for the tube are local buckling for small inversion radii and necking for large inversion radii.
- The ranges where the different failures take place are:

1. $R \leq 0.8$ mm → Local buckling at the top of the tube.
2. $0.8 < R < 3$ mm → Inversion, with a limit displacement for the upper die. Otherwise, local buckling will appear.
3. $3 \leq R \leq 10$ mm → Successful inversion. Potential mode of failure will be that the tube bumps with itself.
4. $R \geq 11$ mm → Necking before the inversion process.

All the results obtained have been purely numerical except those from R=0.5, 5 and 20 mm inversion radii. In order to validate the forming limits radii, it will be interesting to prove these results in an experimental way.

Another possibility is to study the ductile damage for the inversion process due to, as it has been proved, the damage for this process is bigger than the value for the expansion process. This would generate new possibilities in terms of inversion processes.

5. References

A.J. Martínez-Donaire et al. (2018). Analysis of the influence of stress triaxiality on formability of hole-flanging by single-stage SPIF. *International Journal of Mechanical Sciences*.

Análisis de los Procesos de Conformado de Chapa. (n.d.). *Ampliación de Tecnología de Fabricación*.

AutoForm: Forming Reality. (n.d.). Retrieved from https://www.autoform.com/en/glossary/springback/

B. Lossen et al. (2018). Friction-spinning—Grain structure modification and the impact on stress/ strain behaviour. *Journal of Materials Processing Tech*.

C. Becker et 254 al. (2014). Fundamentals of the incremental tube forming process. *CIRP Annals - Manufacturing Technology*.

C. Becker et al. (2014). Fundamentals of the incremental tube forming process. *CIRP Annals - Manufacturing Technology 63* , 253-256.

Cristino et al. (2019). A digital image correlation based methodology to characterize formability in tube forming. *Journal of Starin Analysis*, 139-148.

Cristino et al. (2019). Theory of single point incremental forming of tubes.

D. Cooper. (n.d.). Sheet Metal Forming. *Massachusetts Institute of Technology*.

Dietzel Hydraulik. (n.d.). Retrieved from https://www.dietzel-hydraulik.de/en/products/thin-walled-tubes/overview/

Friction-spinning - Grain structure modification and the impact on stress/strain behaviour. (2018). *Journal of Materials Processing Technology 261*, 242-250.

G. Centeno et al. (2016). Towards the characterization of fracture in thin-walled tube forming. *International Journal of Mechanical Sciences 119*, 12-22.

G. Centeno et al. (2017). On The Utilization of Circle Grid Analysis in Thin-walled Forming of Tubes. *Procedia Engineering 207*, 1773-1778.

G.S. Sekhon et al. (2003). An analysis on external inversion of round tubes. *Journal of Materials Processing Technology 133*, 243-356.

J. Jeswiet et al. (2008). Metal forming progress since 2000. *CIRP Annals - Manufacturing Technology*.

J.P. Magrinho, M.B. Silva, & and G. Centeno et al. (2019). On the determination of forming limits in thin-walled tubes. *International Journal of Mechanical Sciences*.

Magrinho et al. (2019). On the Determination of Forming Limits in Thin-Walled Tubes. *International Journal of Mechanical Sciences*.

Magrinho et al. (2019). On the formability limits of thin-walled tube inversion.

Mariño, S. (2015, Noviembre). Procesos de fabricación de tubos. Maracaibo, República Bolivariana de Venezuela.

P.A. Rosa et al. (2004). Internal inversion of thin-walled tubes using a die: experimental and theoretical investigation. *International Journal of Machine Tools & Manufacture 44*, 775-784.

P.A.R. Rosa et al. (2003). External inversion of thin-walled tubes using a die: experimental and theoretical investigation. *International Journal of Machine Tools & Manufacture*, 787-796.

S.R. Reid. (1993). *Plastic deformation mechanisms in axially compressed metal tubes used as impact energy absorbers.* Manchester: Pergamon Press Ltd.

S.T.S Al-Hassani, W.Johnson, & W.T. lowe. (1972). Characteristics of inversion tubes under axial loading. *Journal of Mechanical Engineering Science*.

T.L. Anderson. (n.d.). Fracture Mechanics. Fundamentals and Applications. In T.L. Anderson. Taylor & Francis.

Annex A – Matlab Code

MATLAB code to determine the coordinates of the node for the construction of the bottom die:

```
n=10;     % number of division of the radius
r=5;      % inversion radius
A=pi/2;
k=1;
m=n+7;

for j=1:n
    P(n-j+1)= 17.95-
    i*6.5+r*cos((A*j/n)+pi)+i*r*sin((A*j/n)+pi)-
    r*cos(pi)-i*r*sin(pi);
end

M(1)=0+i*0;
M(2)=0-i*50;
M(3)=35-i*50;
M(4)=35+i*imag(P(1));

M(m-2)=17.95-i*6.5;
M(m-1)=17.95-i;
M(m)=16.95+i*0;

for j=5:n+4
    M(j)=P(k);
    k=k+1;
end

realpart=real(M);
imaginarypart=imag(M);

for j=1:m
POINTS=fopen('archivo2.txt','wt');
fprintf(POINTS,'\n %f',realpart);
fprintf(POINTS,'\n %f',imaginarypart);
end
    winopen('archivo2.txt')
```

Annex B – Ductile damage and state of the tube at the beginning of the inversion

R_{inv}= 5 mm – Displacement of the upper die: 14.5 mm

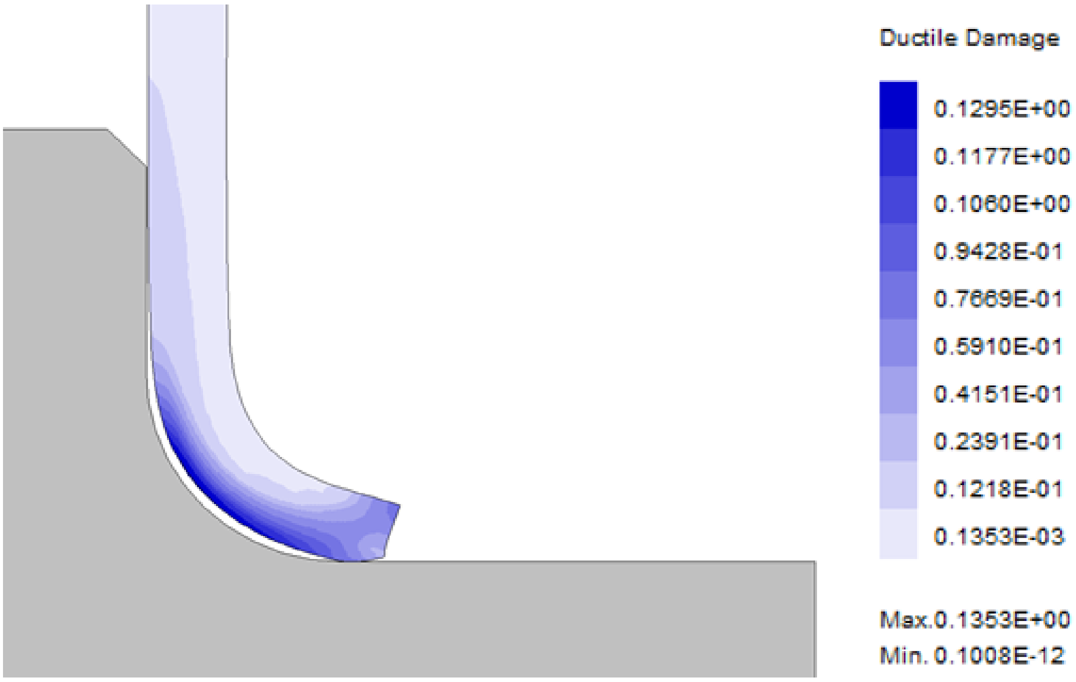

R_{inv}= 6 mm – Displacement of the upper die: 16 mm

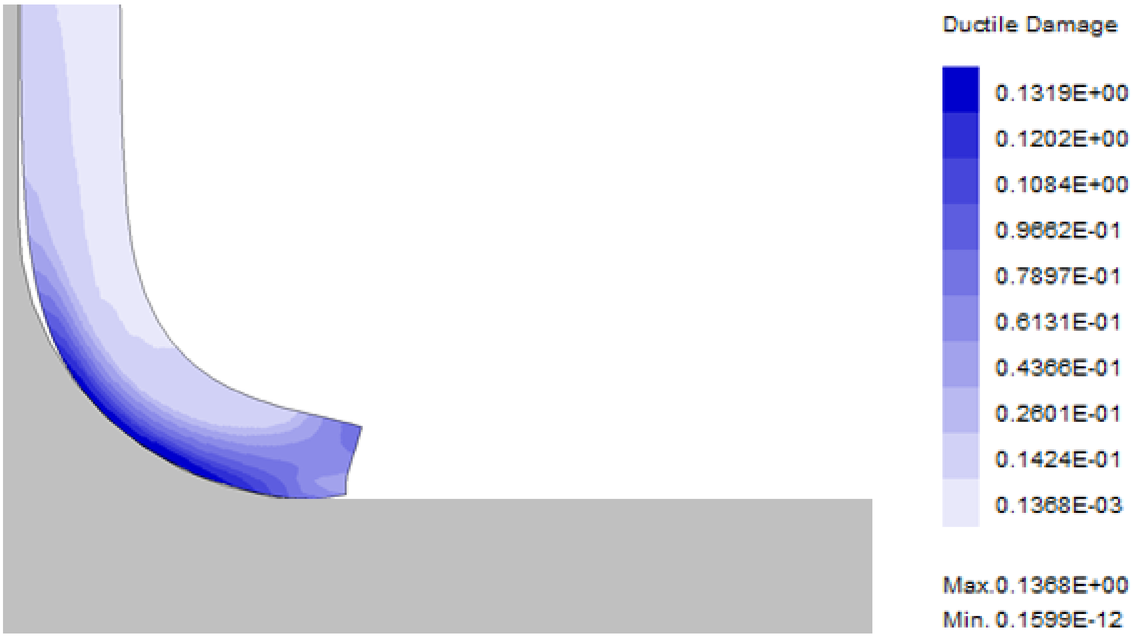

R_{inv}= 7 mm – Displacement of the upper die: 17.5 mm

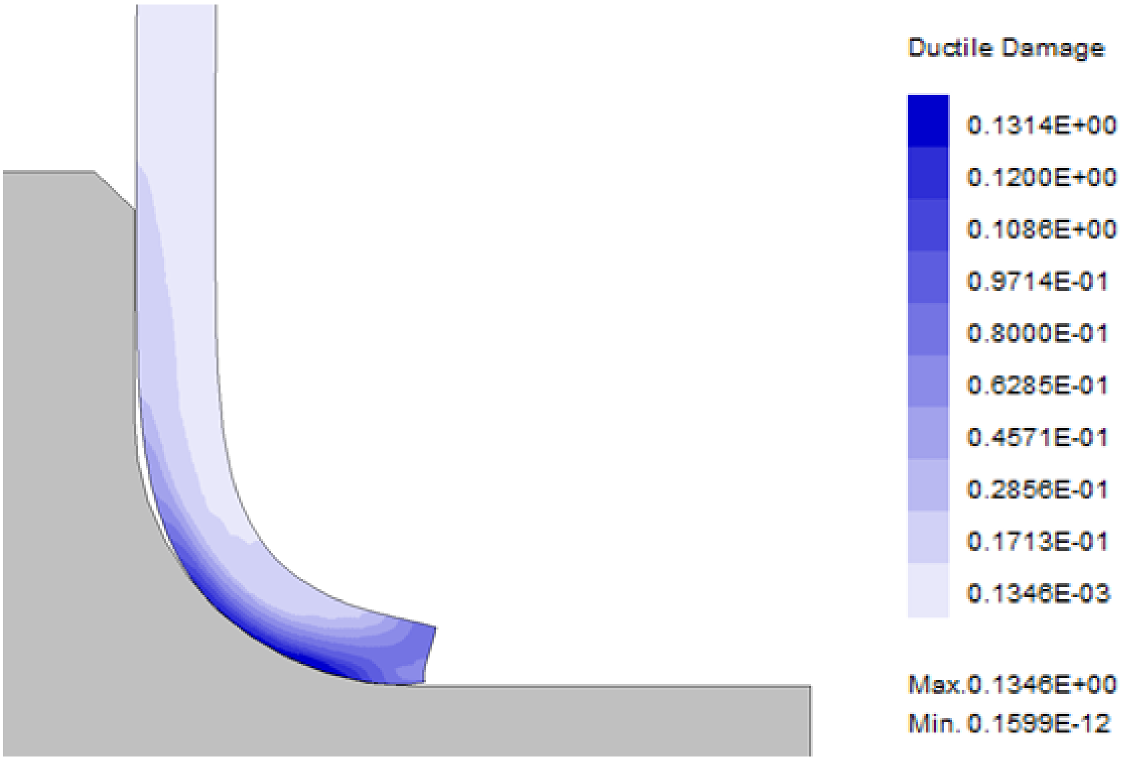

R_{inv}= 8 mm – Displacement of the upper die: 19.5 mm

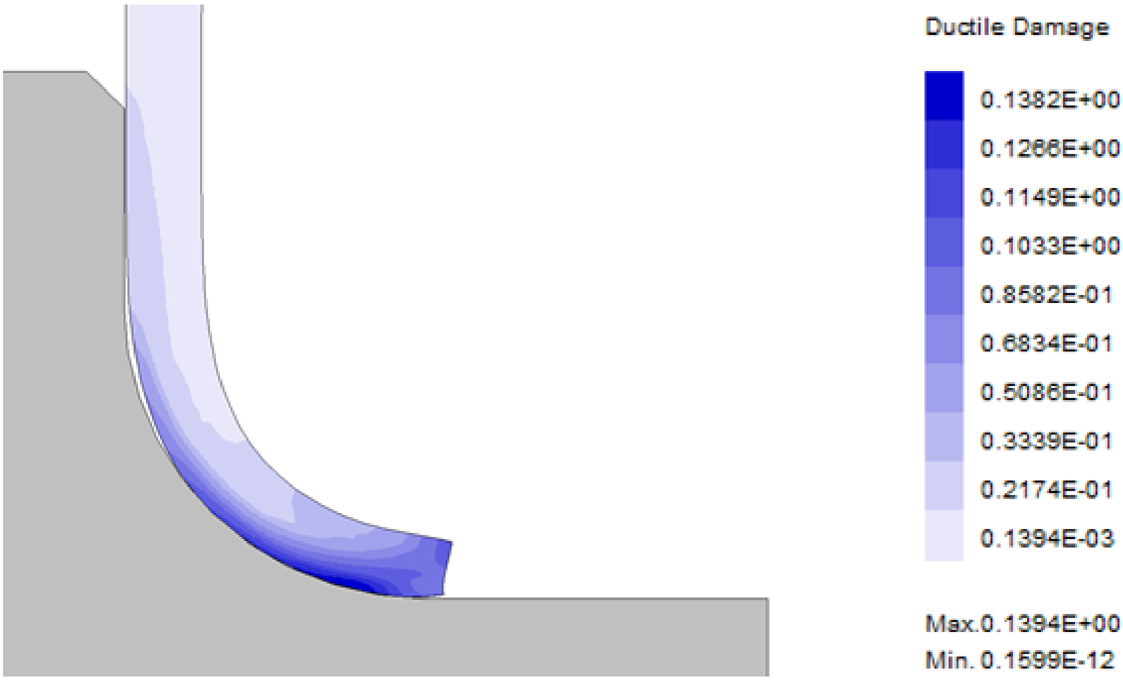

R_{inv}= 9 mm – Displacement of the upper die: 20.8 mm

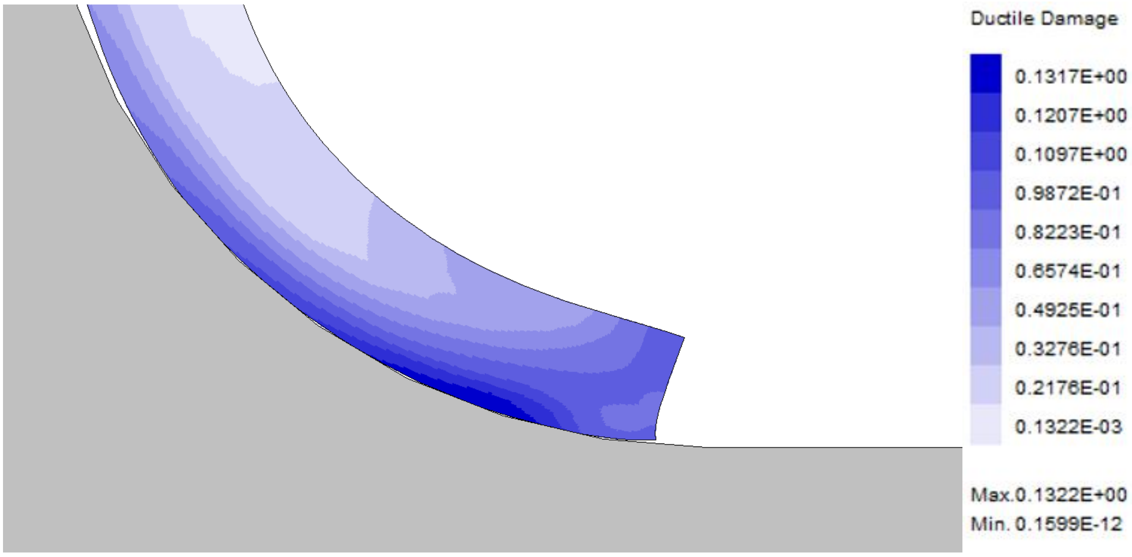
Ductile Damage
0.1317E+00
0.1207E+00
0.1097E+00
0.9872E-01
0.8223E-01
0.6574E-01
0.4925E-01
0.3276E-01
0.2176E-01
0.1322E-03
Max.0.1322E+00
Min. 0.1599E-12

R_{inv}= 10 mm – Displacement of the upper die: 21.5 mm

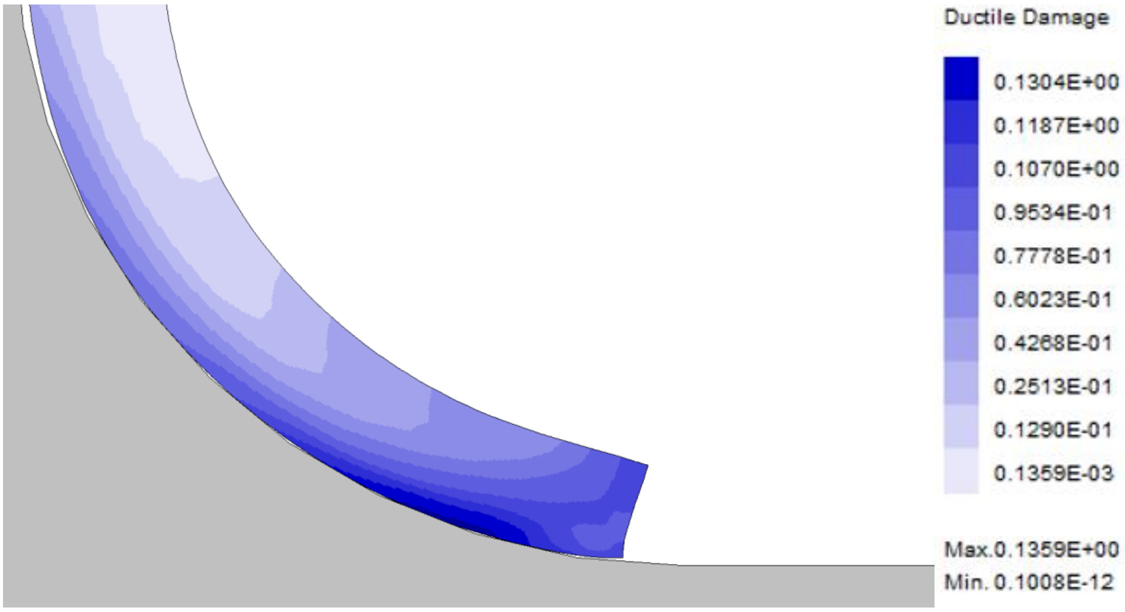
Ductile Damage
0.1304E+00
0.1187E+00
0.1070E+00
0.9534E-01
0.7778E-01
0.6023E-01
0.4268E-01
0.2513E-01
0.1290E-01
0.1359E-03
Max.0.1359E+00
Min. 0.1008E-12

R_{inv}= 11 mm – Displacement of the upper die: 24.5 mm

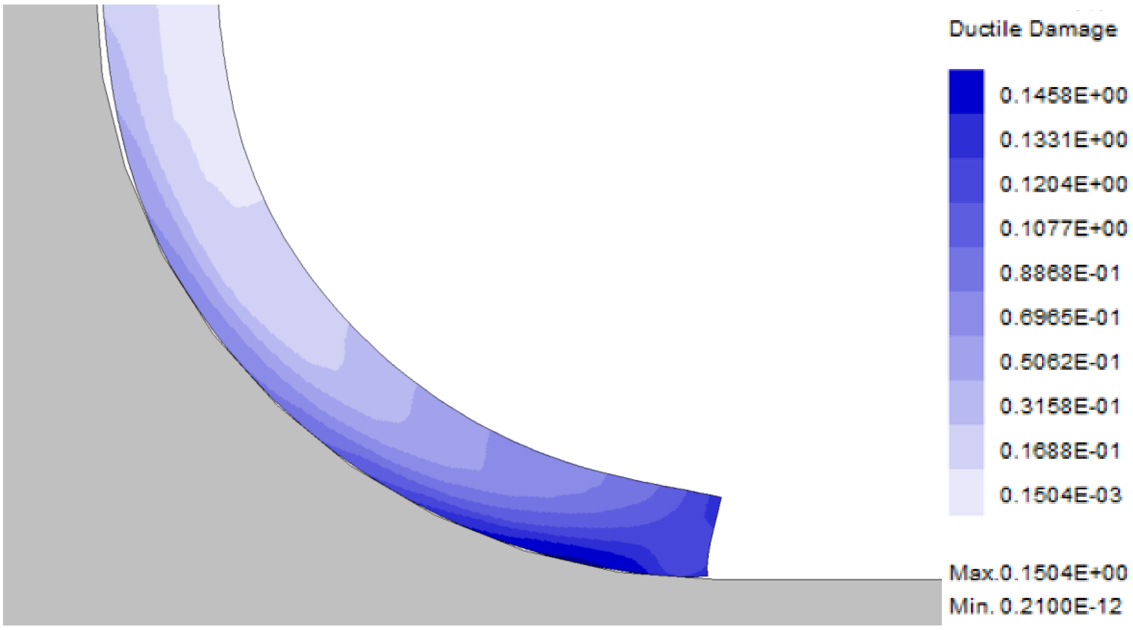

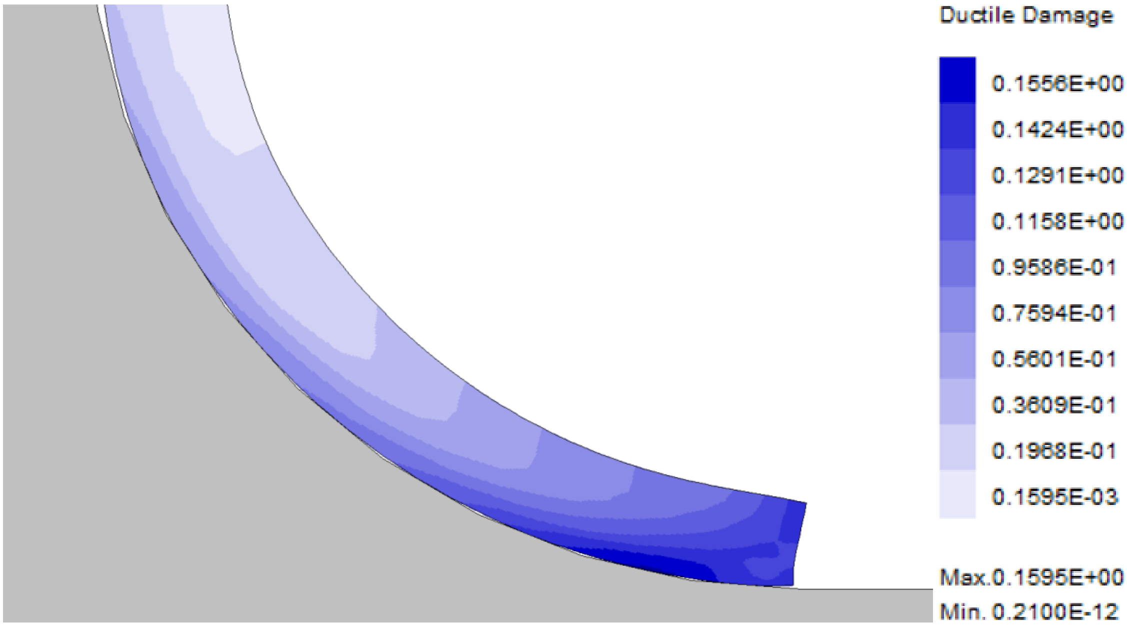R_{inv}= 12 mm – Displacement of the upper die: 26.5 mm